UC Berkeley
UC Berkeley Electronic Theses and Dissertations

Title
CdSe/CdS Tetrapod Quantum Dots as Stress Probes: Characterization, Development, and Applications to Polymer Science and Biophysics

Permalink
https://escholarship.org/uc/item/07k7010f

Author
Olson, Andrew Carl

Publication Date
2014

Peer reviewed|Thesis/dissertation

eScholarship.org Powered by the California Digital Library
University of California

CdSe/CdS Tetrapod Quantum Dots as Stress Probes: Characterization, Development, and Applications to Polymer Science and Biophysics

By

Andrew Carl Olson

A dissertation submitted in partial satisfaction of the

requirements for the degree of

Doctor of Philosophy

in

Chemistry

in the

Graduate Division

of the

University of California, Berkeley

Committee in Charge:
Professor A. Paul Alivisatos, Chair
Professor Peidong Yang
Professor Ronald Gronsky

Spring 2014

Abstract

CdSe/CdS Tetrapod Quantum Dots as Stress Probes:
Characterization, Development, and Applications to
Polymer Science and Biophysics

By

Andrew Carl Olson

Doctor of Philosophy in Chemistry

University of California, Berkeley

Professor A. Paul Alivisatos, Chair

The bulk properties of materials and biological systems depend on their microscale behavior. This is intuitive to chemists who are used to thinking of molecular constituents dictating chemical properties at the macroscale. This bottom-up understanding of materials can be extended to mechanical properties, such as Young's modulus, catastrophic failure modes, which can begin as nanoscale void formation, and polymer chain deformations that occur during mechanical loading. Such fundamental mechanical properties are also crucial in biology, where the viability of an organism is dependent on cell function and behavior. For example, tumorigenesis and metastasis of cancer depends on the ability of a cancerous cell to generate traction forces and move through the body.

This dissertation details recent developments on the tetrapod quantum dot (tQD) as a fluorescence stress probe. The nanometer size and optical properties of the tQD make it uniquely suitable for studying forces and mechanisms of mechanical deformation at the smallest length scales. First, background is provided on colloidal semiconductor quantum dots in general and the tetrapod in particular. Second, development and application of the tQD in synthetic polymer materials is discussed. Third, applications of the tQD as a sensor for cellular biophysics are demonstrated. Finally, further characterization of single tQD properties and future studies are discussed and proposed.

Table of Contents

List of Figures and Tables ..... **ii**

Chapter 1: Introduction
1.1 Colloidal Semiconductor Nanoparticles 1
1.2 Tetrapod Quantum Dots and Lattice Strain 1
1.3 Dissertation Organization 4
References 5

Chapter 2: Tetrapod-Polymer Composites
2.1 Importance of Nanoparticle-Polymer Composites 7
2.2 Uniaxial Deformation of Polymers 7
2.2.1 Mechanisms of Deformation 8
2.2.2 Techniques for Probing Local Deformations 10
2.3 Electrospun Poly Lactic Acid Tetrapod Fibers 10
2.3.1 Fluorescence Monitoring of Tensile Deformation 11
2.3.2 Concentration Dependence on Optical Response 12
2.3.3 Incomplete Stress Transfer to the Nanoparticle Phase 14
2.3.4 Stress Relaxation 15
2.3.5 Cyclic Deformation 15
2.4 Demonstration of Versatility and Robustness 17
2.5 Effects on Composite Mechanical Properties 20
2.6 Conclusions and Future Studies 21
References 22

Chapter 3: Tetrapods as Biological Sensors
3.1 Forces at the Cellular Level - Mechanoreciprocity 26
3.2 Collagen and Tumorigenesis 27
3.3 Tetrapods and Cellular Forces 29
3.3.1 Tetrapod-Collagen Composites 30
3.4 Future Studies 32
3.4.1 Molecular Restructuring of the ECM 32
3.4.2 Biologically Relevant Cell Force Measurements 34
References 36

Chapter 4: Single Particle Studies of Tetrapods
4.1 Fluorescence Studies of Single Tetrapods 38
4.2 Combined AFM-Fluorescence Studies 40
4.2.1 Instrumentation, Procedures, and Pitfalls 41
References 44

Chapter 5: Concluding Remarks **45**

Appendix **46**

List of Figures and Tables

Figure 1.1 Fluorescence, absorbance, and TEM of CdSe/CdS tetrapods....2
Figure 1.2 Previous demonstrations of tQD fluorescence response to pressure 4

Figure 2.1 Polymer stress-strain curve....8
Figure 2.2 Semicrystalline polymer deformation mechanisms....9
Figure 2.3 Electrospinning process and TEM of PLLA-tQD fibers 11
Figure 2.4 Optical and mechanical characterization of PLLA-tQD fibers....13
Figure 2.5 Stress relaxation in PLLA-tQD fibers....16
Figure 2.6 Hysteresis curves of PLLA-tQD fibers....17
Figure 2.7 Optical and mechanical characterization of SEBS-tQD fibers....19

Table 2.1 Properties and structures of demonstrated tQD-compatible polymers 18

Figure 3.1 Structure of collagen....28
Figure 3.2 tQDs as sensors of cardiomyocyte beating....29
Figure 3.3 Setup for simultaneous mechanical and optical measurements....31
Figure 3.4 Characterization of collagen-tQD gels....32
Figure 3.5 Characterization of collagen-PLLA-tQD composite gels....33

Figure 4.1 Irregularities in fluorescence responses....38
Figure 4.2 Spatially indirect emission in tQDs 40
Figure 4.3 Schematic of combined AFM-fluorescence setup 41
Figure 4.4 Spectral wandering and strain-induced fluorescence shifts....42

Figure A1.1 Stress relaxation decay curves fit to exponentials 48
Figure A1.2 Mechanical properties of SEBS-nanoparticles composites 49

Table A1.1 Statistics on fluorescence shifts and concentration....49
Table A1.2 Mechanical properties of PLLA-tQD composites 50

Chapter 1: Introduction

1.1 Colloidal Semiconductor Nanoparticles 1
1.2 Tetrapod Quantum Dots and Lattice Strain 1
1.3 Dissertation Organization 4
References 5

1.1 Colloidal Semiconductor Nanoparticles

Nanoparticles exhibit interesting properties due to their size and consequent nature as quantum-confined materials. Quantum-confined materials can be thought of as belonging to a transition from large molecule to extended solids. Consequently, nanoparticles can be used as a means to study the interactions of molecular-level phenomena with material surfaces such as in charge transport and transfer kinetics[1-3]. Nanoparticles can also be used to study the surface-dependent behaviors of bulk materials as a greater proportion of atoms reside on the nanoparticle surface relative to the interior. Their small size offers a means to study and control facet-specific catalytic events[4], phase transitions[5-7], and the effects of defect sites on material properties[8-10].

The unique properties of nanoparticles and their dependence on the local environment also provide a straight-forward route to study potentially inaccessible nano and micrometer-scale events. Nanoparticles have been demonstrated as sensors for biological events[11-13], gases[14], and the presence of chemicals[15-17].

In this work, we restrict our discussion to the relatively narrow class of colloidal cadmium chalcogenide nanoparticles, commonly known as quantum dots. Optically, these particles are characterized by broad absorption above the bandgap of the semiconductor, narrow emission spectra, and high quantum yields. The unique optical properties of quantum dots are due to their size being similar to the radius of the exciton generated in absorption events, which results in discrete energy states near the bandgap. As a semiconductor material decreases in size, the Bohr radius, r_B, of the exciton becomes spatially confined by the crystal lattice boundaries[18,19]. This relation is approximated as $r_B = a_0\varepsilon/m^*$ where a_0 is the classical radius, approximately 0.53Å, ε is dielectric constant of the material, and m* is the reduced effective mass of the electron/hole pair. Consequently, quantum-confinement is readily observed in materials with large dielectric constants and small effective masses such as cadmium chalcogenides.

Due to the confinement of the electron wavefunction, the optical properties are also highly dependent on any changes to the crystal lattice of the particle. Mostly famously, as a quantum dot decreases in size, the exciton increases in energy. These sorts of effects need not be limited to synthetic procedures resulting in fairly static optical properties in a nanoparticle. Distortions to the crystal lattice of an existing quantum-confined material will result a change in the electronic environment for the exciton.

1.2 Tetrapod Quantum Dots and Lattice Strain

The electronic structure of two quantum-confined materials can be coupled through a shelling reaction. Coupled structures are achieved by combining materials in which the electron potential in the shell is below the vacuum level (or the dielectric of a typical solvent) but above the core's

potential. As discussed above, a change to the lattice of a quantum dot will result in a modified electronic structure of the material. In core/shell structures, this is observed through a shifting of excitonic features to lower energy wavelengths (Figure 1.1A), as the exciton is less confined[18]. In type I structures, the shell material has a larger band gap than the core and causes the exciton to be completely confined to the shell. This isolates the exciton from many of the potential trap states and can be used to reach quantum yields well in excess of 50%[20,21]. The main commercial applications of quantum dots, as biological tags and in displays, utilize the fluorescence properties emergent from a shelled particle.

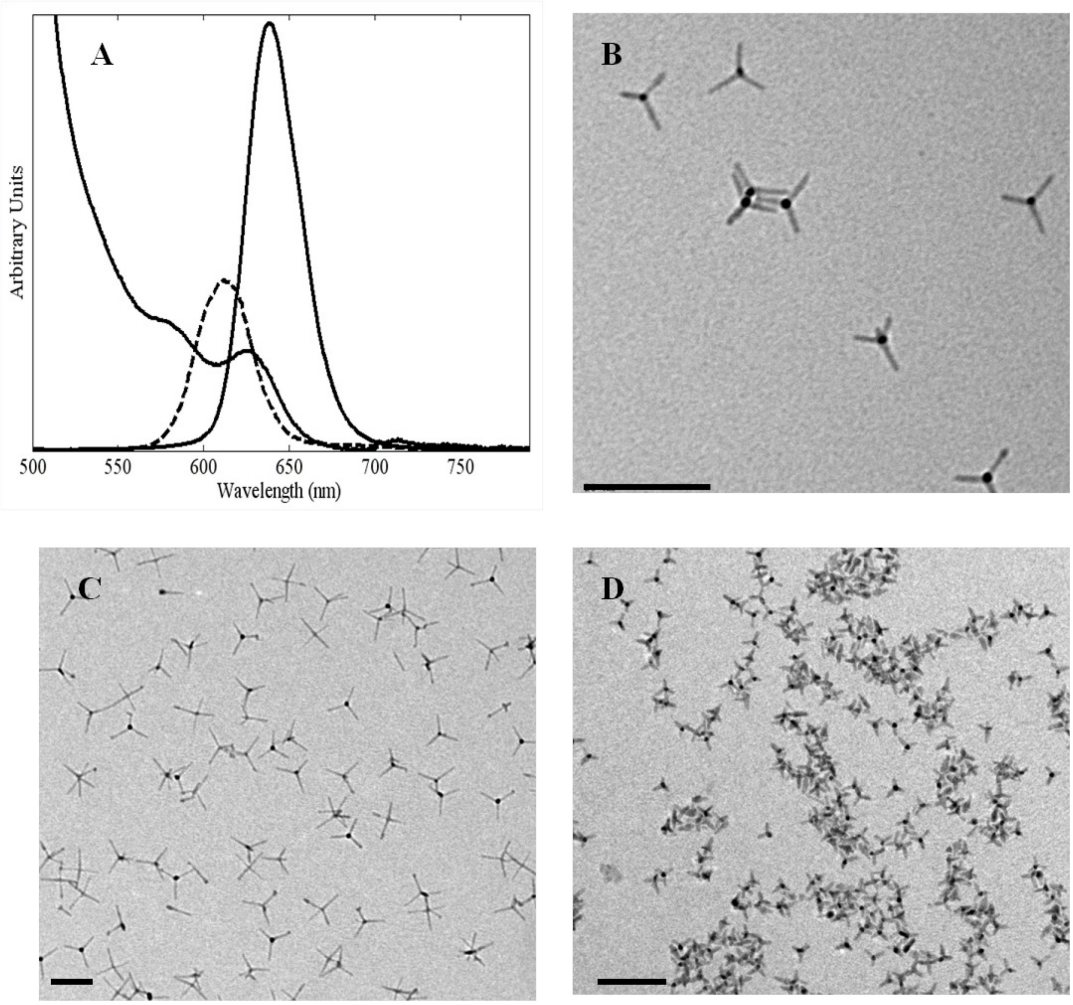


Figure 1.1 - Fluorescence, absorbance, and TEM of CdSe/CdS tetrapods of varying sizes. (A) UV-Vis aborbance and fluorescence of tetrapods (solid line) after growth from CdSe seeds (dotted line). (B) Tetrapods with average arm lengths of 25 nm. (C) Arms of 43 nm. (D) Arms of 15 nm. Scale bar is 100 nm for all images.

Shelling reactions also provide a synthetic means of varying a quantum dot's shape beyond the traditional sphere-like geometry to one-dimensional shapes (nanorods) and a variety of three-dimensional branched particles (tetrapods, dendritic formations, yolk-shell particles, and snowflakes among others)[22-24]. The work here focuses on CdSe/CdS core/shell tetrapods, also referred to as tetrapod quantum dots (tQDs).

Tetrapod quantum dots are synthesized in a two-step seeded growth reaction. A cubic zinc-blende phase CdSe core is grown by careful control of the reaction temperature and passivation of crystal facets by alkylphosphonate ligands. The resulting CdSe seed has four (111) facets. Epitaxial growth of würtzite-phase CdS arms off the (111) facets is performed in a secondary reaction and displays a beautiful symmetry analogous to a methane molecule (Figure 1.1). This is possible due to the small lattice mismatch between select CdSe and CdS planes[25]. This synthetic route also allows for straight-forward control of tetrapod arm dimensions from 15 nm to 50 nm by varying the amount of CdS precursor in the second step of the reaction (Figure 1.1B-D). There are several other methods for synthesizing tetrapods of varying materials but all depend on the nucleation of a cubic phase followed by growth of a hexagonal arm[26-28].

Wang and coworkers used a semi-empirical model to find that nanocrystal shape plays a major role in the electronic and optical wavefunctions of the nanoparticle[29]. This naturally leads to the idea that the mechanical and optical properties of nanoparticles are inherently linked. Further studies using these methods by Schrier, et al, predicted a decreasing bandgap with applied strain in the instance of compressing a single arm of a CdTe tetrapod[30]. Conversely, in the case of applied isotropic compression a tetrapod, like most other quantum dots, will exhibit an increasing bandgap as the increasing physical confinement causes greater overlap in the exciton wave functions[31,32]. The red-shifting (anisoptropic) fluorescence behavior can be attributed to the splitting of the CdSe valence band, which is comprised of the Se $4p_{xyz}$ orbitals. As the CdS arm transfers stress to the CdSe core, the symmetry of the particle's lattice is broken, and one of the 4p orbitals will decrease in energy as the net result of the bond stretching and compressing in the core.

In 2009, this behavior was experimentally verified and proven to be unique to the tetrapod structure by studies from Choi, et at, in the Alivisatos group[33]. Spherical quantum dots, nanorods, and tetrapods were subjected to hydrostatic and nonhydrostatic pressures in a diamond-anvil cell experiment. Tetrapods were shown to be unique in their ability to differentiate hyrostatic and nonhydrostatic pressures through blue shifting and red shifting fluorescence, respectively. The red-shifting response of tetrapods was shown to monotonically increase with increasing pressure (Fig. 1.2A).

More recently, tQDs were demonstrated as optical strain gauges with micrometer spatial resolution in synthetic polymers (Figure 1.2B)[34]. This work also made use of the easily controlled dimensions of the tQD to optimize nanoparticle dimensions for a maximum fluorescence response. It was found that approximately 25 nm CdS arms are the optimal size for tQDs as sensors in the case of 5 nm CdSe core. This is attributed to a decreased stress transfer to the particle from the polymer phase as the arms become smaller. There is less interface to provide stress transfer from the polymer to the same size core as compared to larger arms. In the case of large, 40 nm, arms, the response was also less than that of 25 nm arms. This is likely due to stress concentration at stacking faults in the arms as defects become more prevalent in larger structures. Since the exciton is largely confined to the CdSe core, stress concentrators in the CdS arms are less likely to induce large optical shifts than stresses that are transferred to the core. Further aspects of this study are discussed in Chapter 2.

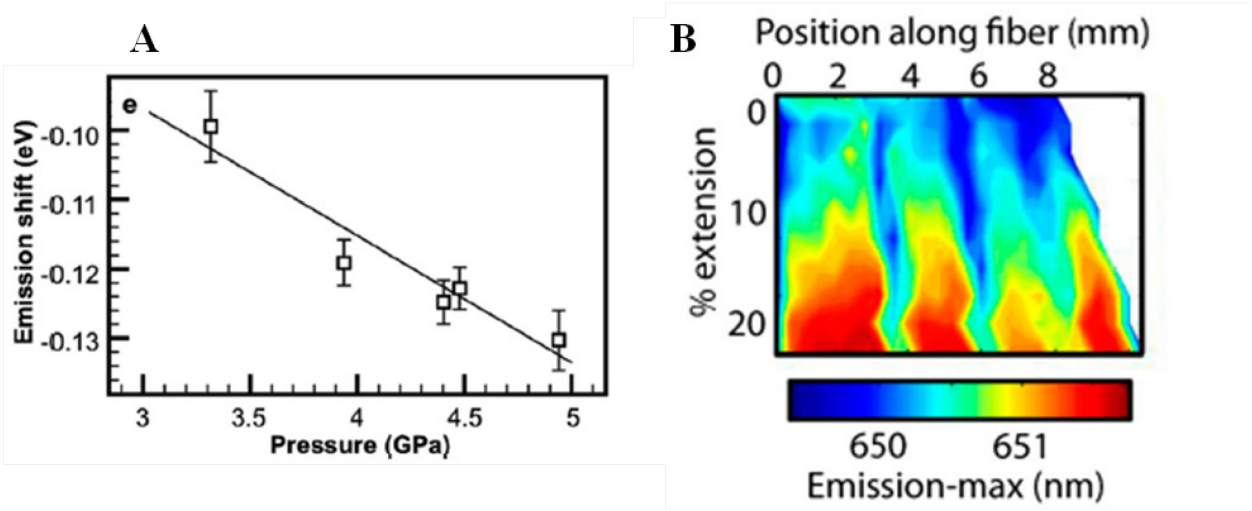


Figure 1.2: Previous experiments on tetrapods and pressure. (A) Tetrapods in a diamond-anvil cell experiment were suspended in a nonhydrostatic medium to validate theoritical predictions. (B) In a separate experiment, tQDs were first demonstrated as strain gauges capable of measuring homogeneity in the microscale response of polymers to mechanical deformation. Figures adapted from References 33 and 34.

1.3 Dissertation Organization

The work presented in this dissertation builds on the theoretical models and proof of concept experiments that demonstrated the potential of tQD as a means to investigate nanoscale forces. Chapter 2 discusses tQD-polymer composites. This includes a review of the deformation mechanisms in polymers that occur at the molecular and nanometer level during bulk material deformations. The tetrapod is then introduced as a means to interrogate those mechanisms as well as provide otherwise inaccessible phase-specific information on stress-transfer in a composite material. Comparison between fluorescence microscopy studies and traditional bulk mechanical measurements of tQD-polymer composites under uniaxial strain provide further verification and details of the unique sensing ability of the tQD. These comparisons are extended to a number of testing parameters – stress relaxation and cyclic loading – and widely differing polymers in order to demonstrate the robust and versatile nature of the tQD sensor. Finally, chapter 2 concludes with a study comparing the Young's modulus in composites with branched and unbranched nanoparticle fillers.

In chapter 3, potential applications to cell and cancer biophysics are explored. A brief overview of mechanical forces at the cellular level in living organisms is provided. Direct and indirect methods of cellular force measurement are studied in which cells exert force directly on the tQD and strain their surrounding composite matrix, respectively. Finally, future studies on the importance of quantifying and investigating these forces are proposed.

Throughout the studies in chapters 2 and 3, interesting results are seen which are beyond our current understanding of the relationship between the tQD electronic structure and applied strains. Single particle combination AFM-fluorescence experiments are discussed in chapter 4. These experiments are discussed in the context of providing an increased fundamental understanding of the tQD and how that might be applied to future studies of polymer and biological forces.

Chapter 1 References

1. Ginger, D. S.; Greenham, N. C., Charge injection and transport in films of CdSe nanocrystals. *Journal of Applied Physics* 2000, 87, 1361-1368.
2. Scheele, M.; Engel, J. H.; Ferry, V. E.; Hanifi, D.; Liu, Y.; Alivisatos, A. P., Nonmonotonic Size Dependence in the Hole Mobility of Methoxide-Stabilized PbSe Quantum Dot Solids. *ACS nano* 2013, 7, 6774-6781.
3. Huynh, W. U.; Dittmer, J. J.; Alivisatos, A. P., Hybrid nanorod-polymer solar cells. *science* 2002, 295, 2425-2427.
4. Somorjai, G. A.; Li, Y., Major successes of theory-and-experiment-combined studies in surface chemistry and heterogeneous catalysis. *Topics in Catalysis* 2010, 53, 311-325.
5. Grünwald, M.; Lutker, K.; Alivisatos, A. P.; Rabani, E.; Geissler, P. L., Metastability in pressure-induced structural transformations of CdSe/ZnS core/shell nanocrystals. *Nano letters* 2012, 13, 1367-1372.
6. Polking, M. J.; Jain, P. K.; Bekenstein, Y.; Banin, U.; Millo, O.; Ramesh, R.; Alivisatos, A. P., Controlling localized surface plasmon resonances in GeTe nanoparticles using an amorphous-to-crystalline phase transition. *Physical review letters* 2013, 111, 037401.
7. Tolbert, S. H.; Alivisatos, A. P., Size dependence of a first order solid-solid phase transition: the wurtzite to rock salt transformation in CdSe nanocrystals. *Science*, 373-373.
8. Engel, J. H.; Surendranath, Y.; Alivisatos, A. P., Controlled Chemical Doping of Semiconductor Nanocrystals Using Redox Buffers. *Journal of the American Chemical Society* 2012, 134, 13200-13203.
9. Herhold, A. B.; Chen, C.-C.; Johnson, C. S.; Tolbert, S. H.; Alivisatos, A. P., Structural transformations and metastability in semiconductor nanocrystals. *Phase Transitions* 1999, 68, 1-25.
10. Dalpian, G. M.; Chelikowsky, J. R., Self-purification in semiconductor nanocrystals. *Physical review letters* 2006, 96, 226802.
11. Bruchez, M.; Moronne, M.; Gin, P.; Weiss, S.; Alivisatos, A. P., Semiconductor nanocrystals as fluorescent biological labels. *Science* 1998, 281, 2013-2016.
12. Alivisatos, P., The use of nanocrystals in biological detection. *Nature biotechnology* 2004, 22, 47-52.
13. Sönnichsen, C.; Reinhard, B. M.; Liphardt, J.; Alivisatos, A. P., A molecular ruler based on plasmon coupling of single gold and silver nanoparticles. *Nature biotechnology* 2005, 23, 741-745.
14. Liu, N.; Tang, M. L.; Hentschel, M.; Giessen, H.; Alivisatos, A. P., Nanoantenna-enhanced gas sensing in a single tailored nanofocus. *Nature materials* 2011, 10, 631-636.
15. Frasco, M. F.; Chaniotakis, N., Semiconductor quantum dots in chemical sensors and biosensors. *Sensors* 2009, 9, 7266-7286.
16. Murphy, C. J., Peer reviewed: optical sensing with quantum dots. *Analytical Chemistry* 2002, 74, 520-A.
17. Costa-Fernández, J. M.; Pereiro, R.; Sanz-Medel, A., The use of luminescent quantum dots for optical sensing. *TrAC Trends in Analytical Chemistry* 2006, 25, 207-218.
18. Rossetti, R.; Ellison, J. L.; Gibson, J. M.; Brus, L. E., Size effects in the excited electronic states of small colloidal CdS crystallites. *The Journal of chemical physics* 1984, 80, 4464-4469.
19. Bányai, L.; Koch, S. W., *Semiconductor quantum dots*. World Scientific: 1993; Vol. 2.

20. Michalet, X.; Pinaud, F. F.; Bentolila, L. A.; Tsay, J. M.; Doose, S.; Li, J. J.; Sundaresan, G.; Wu, A. M.; Gambhir, S. S.; Weiss, S., Quantum dots for live cells, in vivo imaging, and diagnostics. *science* 2005, 307, 538-544.
21. Reiss, P.; Bleuse, J.; Pron, A., Highly luminescent CdSe/ZnSe core/shell nanocrystals of low size dispersion. *Nano letters* 2002, 2, 781-784.
22. Peng, X.; Manna, L.; Yang, W.; Wickham, J.; Scher, E.; Kadavanich, A.; Alivisatos, A. P., Shape control of CdSe nanocrystals. *Nature* 2000, 404, 59-61.
23. Milliron, D. J.; Hughes, S. M.; Cui, Y.; Manna, L.; Li, J.; Wang, L.-W.; Alivisatos, A. P., Colloidal nanocrystal heterostructures with linear and branched topology. *Nature* 2004, 430, 190-195.
24. Manna, L.; Scher, E. C.; Alivisatos, A. P., Synthesis of soluble and processable rod-, arrow-, teardrop-, and tetrapod-shaped CdSe nanocrystals. *Journal of the American Chemical Society* 2000, 122, 12700-12706.
25. Talapin, D. V.; Nelson, J. H.; Shevchenko, E. V.; Aloni, S.; Sadtler, B.; Alivisatos, A. P., Seeded growth of highly luminescent CdSe/CdS nanoheterostructures with rod and tetrapod morphologies. *Nano letters* 2007, 7, 2951-2959.
26. Manna, L.; Milliron, D. J.; Meisel, A.; Scher, E. C.; Alivisatos, A. P., Controlled growth of tetrapod-branched inorganic nanocrystals. *Nature materials* 2003, 2, 382-385.
27. Carbone, L.; Kudera, S.; Carlino, E.; Parak, W. J.; Giannini, C.; Cingolani, R.; Manna, L., Multiple wurtzite twinning in CdTe nanocrystals induced by methylphosphonic acid. *Journal of the American Chemical Society* 2006, 128, 748-755.
28. Yu, W. W.; Wang, Y. A.; Peng, X., Formation and stability of size-, shape-, and structure-controlled CdTe nanocrystals: ligand effects on monomers and nanocrystals. *Chemistry of Materials* 2003, 15, 4300-4308.
29. Schrier, J.; Lee, B.; Wang, L. W., Mechanical and electronic-structure properties of compressed CdSe tetrapod nanocrystals. *J Nanosci Nanotechnol* 2008, 8, 1994-8.
30. Fang, L.; Park, J. Y.; Cui, Y.; Alivisatos, P.; Shcrier, J.; Lee, B.; Wang, L.-W.; Salmeron, M., Mechanical and electrical properties of CdTe tetrapods studied by atomic force microscopy. *The Journal of chemical physics* 2007, 127, 184704.
31. Wei, S.-H.; Zunger, A., Predicted band-gap pressure coefficients of all diamond and zinc-blende semiconductors: Chemical trends. *Physical Review B* 1999, 60, 5404.
32. Li, J.; Wang, L.-W., Deformation potentials of CdSe quantum dots. 2004.
33. Choi, C. L.; Koski, K. J.; Sivasankar, S.; Alivisatos, A. P., Strain-Dependent Photoluminescence Behavior of CdSe/CdS Nanocrystals with Spherical, Linear, and Branched Topologies. *Nano Letters* 2009, 9, 3544-3549.
34. Choi, C. L.; Koski, K. J.; Olson, A. C. K.; Alivisatos, A. P., Luminescent nanocrystal stress gauge. *Proceedings of the National Academy of Sciences* 2010, 107, 21306-21310.

Chapter 2: Tetrapod-Polymer Composites

2.1 Importance of Nanoparticle-Polymer Composites....7
2.2 Uniaxial Deformation of Polymers....7
2.2.1 Mechanisms of Deformation....8
2.2.2 Techniques for Probing Local Deformations....10
2.3 Electrospun Poly Lactic Acid Tetrapod Fibers....10
2.3.1 Fluorescence Monitoring of Tensile Deformation....11
2.3.2 Concentration Dependence on Optical Response....12
2.3.3 Incomplete Stress Transfer to the Nanoparticle Phase....14
2.3.4 Stress Relaxation....15
2.3.5 Cyclic Deformation....15
2.4 Demonstration of Versatility and Robustness....17
2.5 Effects on Composite Mechanical Properties....20
2.6 Conclusions and Future Studies....21
References....22

2.1 Nanoparticle-Polymer Composites

Polymer nanocomposites display a number of useful properties that are enhanced compared to either individual constituent of the material. Typically, these enhancements are thought of in terms of the properties of the polymer matrix and include enhanced ductility, shear and bulk modulus, optical properties, conductive properties, thermal conductivity, antimicrobial properties, and biocompatibility among many others[1]. Alternatively, the polymer matrix can be thought of as a means of more easily integrating nanoparticles into otherwise inaccessible environments such as the cellular cytoplasm through polymer vesicles[2].

The interface between nanoparticles and polymers during the application of macroscopic mechanical forces is one of the most important factors in determining bulk composite mechanical properties. The interface dictates the fundamental mode of any interaction between the composite phases. In the case of stress-transfer, this could mean catastrophic failure of the bulk material or the loss of transfer of the desired property from the particle to the polymer. Stress transfer can also be used as a means of mechanically activating properties of a mechanophore such as cis/trans isomerization or lowering of the activation barrier for other chemical transformations[3].

However, rational design of these materials has remained elusive, due to a lack of detailed understanding of stress profiles at the microscale and nanoscale. In this work, we demonstrate and further develop the tetrapod quantum dot (tQD) as a means of probing the nanoparticle-polymer interface in advanced composites.

2.2 Uniaxial Deformation of Polymers

When a polymer is strained at a macroscopic level, there are many mechanisms of deformation that occur in the internal structure of the material. The optical readout from a tetrapod strain gauge is a summation of all of the modes of deformation that result in a strain in the tetrapod structure. That simplification of mechanical information to an optical signal is advantageous as it

provides a way to measure the stress transfer to only the particle-phase of a composite in a convoluted system.

2.2.1 Mechanisms of Deformation

In this study, polymer composites were uniaxially extended in tensile tests. A typical stress-strain curve for a film of an elastomeric composite is shown in Figure 2.1. Stress (force per unit area, typically pascals) is a function of applied strain (deformation relative to the original material, unitless). Figure 2.1A illustrates typical true stress-strain curves typical of brittle, plastic, and elastomeric polymers. True stress and strain, as compared to an engineering stress and strain, is defined by the instantaneous cross-sectional area of the sample rather than the original. After the yield point in ductile materials (Fig. 2.1B), necking begins to occur as the local cross-sectional area decreases relative to the rest of the sample. Necking causes a decrease in apparent engineering stress; whereas, the true stress continues to rise with increasing strain. The majority of the work presented here will concern plastic and elastomeric polymers analyzed using engineering stress and strain. Figure 2.1B highlights some of the important aspects of a stress-strain curve. Tensile deformation occurs elastically until the yield point of the material. Continuing application of strain results in plastic deformations as bonds between polymer chains are broken and voids begin to form in the internal structure of the material. Finally, the material fails entirely when a crack propagates across the entire sample.

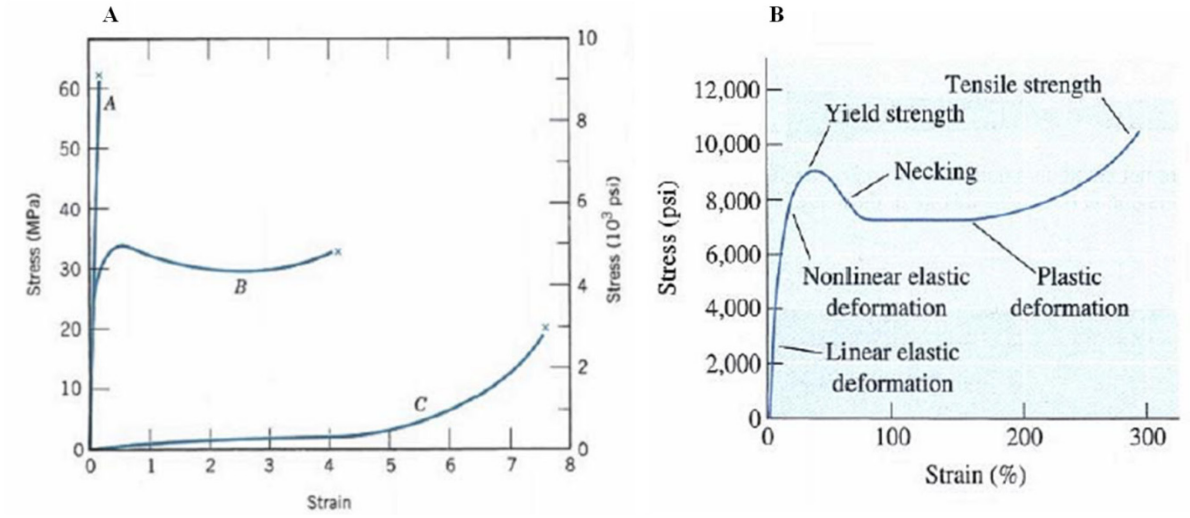


Figure 2.1 – Sress-strain behaviors for typical polymers under tensile testing. (A) Examples of brittle, A, plastic, B, and elastomeric, C, polymers. Note the strain hardening at high strains for the plastic and elastomer cases. (B) Schematic illustrating important definitions for mechanical properties of polymers. Necking refers to the continuing region of deformation after the yield point is reached. Adapted from Reference 4.

At small strains, the resulting stress in the material linearly increases with increasing extension. This is the elastic regime of the material. By definition, all deformations in this regime can be considered entirely recoverable and the underlying mechanism is the mechanical stretching and alignment of the polymer chains with the tensile axis. In semi-crystalline cases, it has become clear that even at small strains there are local plastic events[5]. Once the yield point of the material

is reached, crazing, lamellae reorganization, slipping, fragmentation, localized melting, recrystallization and other plastic deformations dominate the response of the polymer[6]. The combination of these mechanisms results in a real-world response of a polymer that is highly anisotropic at the microscale. AFM studies of poly(1-butene) during tensile drawing found local strains of up to 10% during the macroscopic application of only 6% strain[7].

The following section focuses on the deformation of a semicrystalline polymer, poly lactic acid (PLA). Poly lactic acid is a synthetic biodegradable polymer that has found use in a wide variety of applications including surgical and medical implants[8], compostable packaging[9], and 3D printing[10]. Electrospun PLA has also been shown as potential drug delivery systems[11] and biological scaffolds[12]. The properties of pure PLA fibers have been studied extensively[13-15] making it an ideal system for characterizing the tQD probe and studying its effects on the host matrix. The major deformation mechanisms specific to a semicrystalline polymer are shown in Figure 2.2. In a pure semicrystalline polymer, the application of strain first induces elongation of the molecular chains in the amorphous region (Fig 2.2A). The crystalline regions of the polymer then rotate and reorient along the axis of extension (Fig 2.2B). Further elongation is characterized by plastic deformations and necking described above including void formation and cracking of the lamellae (Fig 2.2C). Finally, a second region of rapidly increasing hardening occurs as the molecular structure has become entirely aligned with the tensile axis (Fig 2.2D).

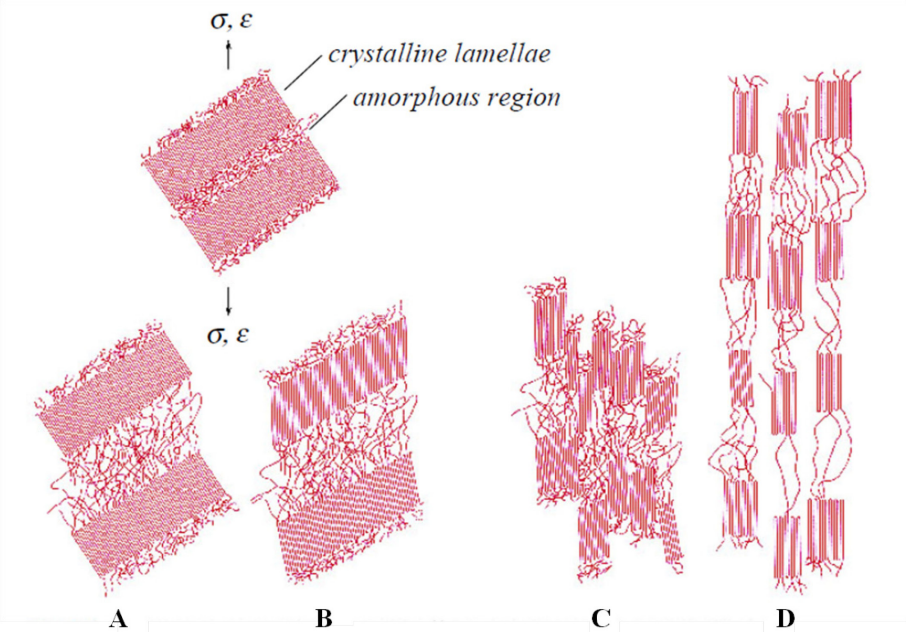


Figure 2.2: Semicrystalline polymer deformation mechanisms. (A) Amorphous chain alignment occurs initially followed by (B) reorientation of crystalline regions. (C) Voids and fracturing of crystalline domains occurs at higher strains. (D) The majority of the polymer structure finally orients in the strain-hardening region during tensile testing. Adapted from Reference 16.

Introducing a nanoparticle, with dimensions similar to those of the mechanisms described above, provides a local probe of these phenomena while also adding a further layer of complexity to an already convoluted response. It is difficult to predict how stress will be transferred to an inclusion in a polymer composite given all of these variables even though a nanoparticle is confined to the amorphous region of a semicrystalline polymer due the relative sizes of the

nanoparticle and the lamellae domains. However, as discuss in previous sections, the strain-state of a particle can have a large impact on its properties. In order to design, engineer, and utilized potential advanced nanoparticle-polymer materials, it would be ideal to have a way to measure only those local deformation mechanisms that affect the particle phase of the composite.

2.2.2 Techniques for Probing Local Deformations

Rational design of nanoparticle-polymer composites has remained elusive, due to a lack of detailed understanding of stress profiles at the microscale and nanoscale. Specifically, an understanding of the interface between the filler and polymer, how stresses are transferred across that barrier, and the actual loading conditions in the composite as compared to the isostrain case are critical in reproducibly synthesizing composites[17-19].

Established techniques for these studies - including micro-Raman spectroscopy[20], synchrotron radiation[21], and electron backscattering[22] as well as contact techniques such as atomic force microscopy[23,24], nanoindentation[25], and others[26] - are difficult to adapt to *in vivo*stress detection and premature failure detection in service due to their stringent requirements in sample size and shape or need for controlled laboratory environments. Recent advances in smart materials have used self-reporting fillers such as near-infrared molecular probes[27], micrometer-sized ZnO tetrapods[28], metal nanoparticles[29,30], and bioinspired concentric optical fibers with varying refractive index[31]. However, these fillers have drawbacks, including altering the molecular-level composition and structure of the polymer and potentially weakening multiple mechanical properties such as toughness. It is therefore of considerable interest to develop an optical luminescent stress sensing nanoparticle, and to establish ways of embedding these inside polymers without perturbing the mechanical properties that are being sensed. Herein, we demonstrate that it is possible to use luminescent semiconductor nanocrystal tetrapods as optical stress sensors.

2.3 Electrospun Poly Lactic Acid Tetrapod Fibers

In this work, nanoparticle-polymer composites are formed through electrospinning. Electrospinning is a versatile technique in which a droplet of polymer solution is suspended in a large electric field. Upon sufficiently high electric field application (typically 1 kV/cm or greater), the droplet loses its spherical shape and begins to elongate, forming a shape termed the Taylor cone[32]. Subsequently, a jet stream erupts from the unstable Taylor cone, forming fibers at the grounded electrode. The large electric field may cause nanocrystals and particle aggregates to be more uniformly dispersed throughout the polymer matrix than other nanocomposite fabrication methods[33,34]. This may minimize the formation of stress concentrations within the nano/microstructure, which would act to degrade the mechanical properties of composite materials[35,36].

As-synthesized tetrapods and a solution of polymer in chloroform are mixed and loaded into a 1-mL syringe with an attached #21 gauge needle. A droplet of the solution is manually ejected from the syringe immediately prior to applying a one kilovolt/centimeter electric field. This causes individual fibers to be formed on the dual rod electrodes (Fig. 2.3A). The fibers dry within seconds and are collected for optical and mechanical tests. Figure 2.3D represents a

bright-field fluorescence image of a resulting poly lactic acid (PLLA) electrospun fiber, showing red 650 nm fluorescence from the tetrapods dispersed throughout the fiber. No diffusion of the fluorescence intensity along the length of the fiber during tests was observed, leading us to conclude that the tetrapods are effectively incorporated into the polymer composite structure. The tetrapods are not covalently bound to the matrix, nor have they undergone ligand exchange. They are simply incorporated into the polymer via electrospinning with their native hydrophobic ligands. For a full description of synthesis, testing parameters, instrumentation, and procedures, please see Appendix.

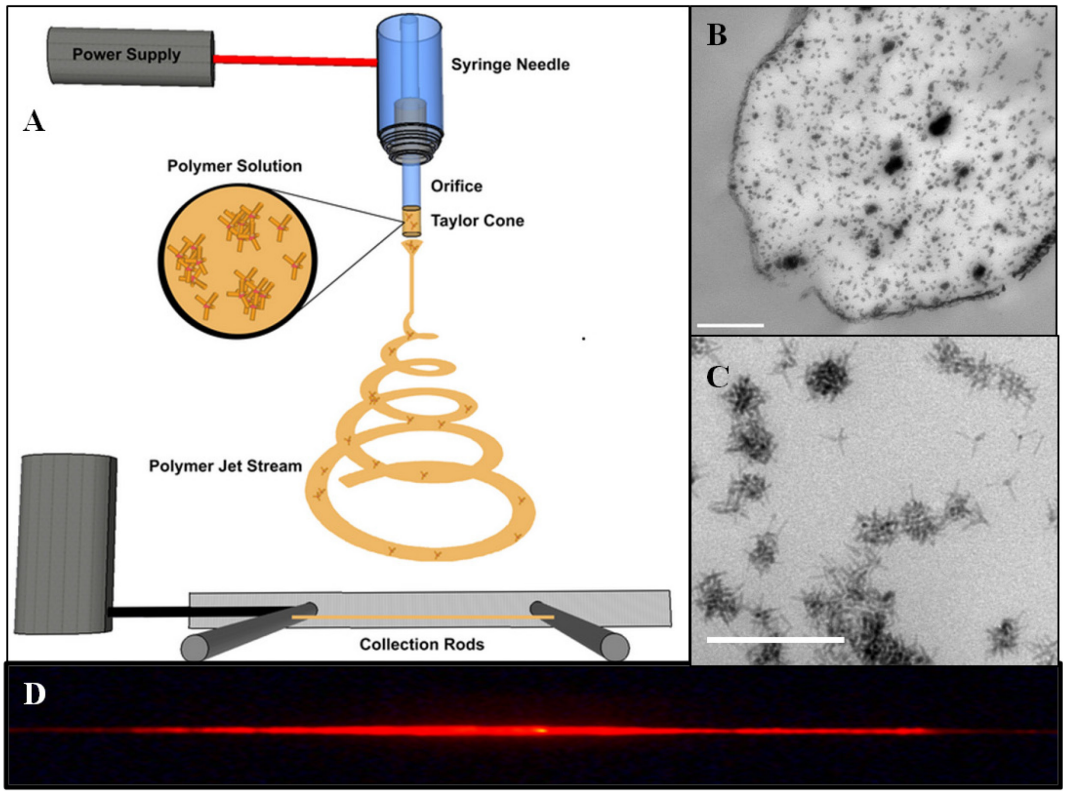


Figure 2.3: (A) Schematic of electrospinning process. (B) TEM image of tQD-PLLA electrospun fiber cross-section (scale bar 500 nm). (C) Higher magnification view of tQD-PLLA composite shown in part C (scale bar 200 nm). (D) Fluorescence image of tQD-PLLA electrospun fiber.

Electrospinning also allows for the easy formation of composites with varying weight percents of particles. Solutions are simply prepared with the desired relative proportions of polymer and tetrapods. For example, tetrapods were incorporated at concentrations of 0, 3.6, 10, 20, and 40% by weight of the PLLA polymer. Parts B and C of Figure 2.3 show the polymer–tetrapod fiber TEM images where the tetrapods are mostly forming aggregates in the fiber. Particles and aggregates show no preference for the PLLA–solvent interface or interior of the fiber, but instead formed evenly throughout the fiber. We have also extended this processing technique to several other polymers as discussed later in this section.

2.3.1 Fluorescence Monitoring of Tensile Deformation

After collection, fibers were mounted onto the piezodrive *in situ* stretcher for fluorescence tests or onto cardboard tabs for mechanical tests on an Agilent T150 Universal Testing Machine

(UTM). Figure 2.4A shows the raw spectra from a typical fluorescence test, indicating both a redshift as well as an increase in the full-width half-maximum (FWHM) of the fluorescence spectrum as a function of stretching. As previously discussed, red-shifts in fluorescence during extension cannot be explained by polymer heating or changes in refractive index[37]. The increase in FWHM (10–20% increase) may be due to a combination of innate spectral line broadening during tetrapod nanocrystal deformation and the natural heterogeneity of strain states within the PLLA polymer fiber. The deformation of the tQD leads to bending of the CdS arms which stretches some bonds more than others; for example, the bonds at the interface between the arm and the CdSe core are more stretched than bonds within the CdSe core[38]. Additionally, as discussed above there is heterogeneity in the local strain state of polymers undergoing tensile deformation. Previous work demonstrated how tetrapods could be used to study strain state variations in fibers on a millimeter scale[37]. Variations on the micrometer scale (the diameter of the laser spot) should also be detectable by a nanometer size load cell. In the absence of single nanocrystal photoluminescence studies in the fibers, it is not yet known to what degree deformation of an individual nanocrystal broadens its emission, so the exact contribution of these mechanisms to the FWHM broadening is unclear. However, local variations in the strain state of the composite structure are likely to dominate intrinsic spectral broadening[37,38].

Regardless, the redshift in peak emission clearly tracks fiber deformation. Figure 2.4B shows the result of fitting the spectra in Figure 2.4A to single Gaussians and then plotting these as a function of strain. It indicates an initial slack region followed by a linear elastic region, which then yields and flattens out into a plastic regime. This result matches textbook polymer tensile test graphs, as well as our own mechanical tests conducted on the same batch of fibers (Figure 2.4D).

2.3.2 Concentration Dependence on Optical Response

Figure 2.4C indicates that as the concentration of tetrapods in the polymer increases, tQD sensitivity to strain in the fiber increases as evidenced by the average slopes of the linear region. Between concentrations of 3.6 to 20% by weight of the tQDs in the polymer, the average fluorescence slope increases 60% from 39 to 62 ΔmeV/strain (averaged for 13 and 12 samples, respectively; see Appendix Table A1.1 for full statistics), though the general shape of the tensile curves is constant. The observed clear distinction between elastic and plastic regimes and consistent curve shape across all particle concentrations in fluorescence tests has not been reported previously[28,37]. Although optical and mechanical tests were conducted on different fibers, all nanocomposite fibers used in comparative tests came from the same batch of electrospun fibers prepared using the same tQDs and polymer precursor solutions.

Fiber-reinforced polymer composite studies help explain the observed concentration-dependence in our analogous system. In fiber-polymer composites, provided the fiber/matrix interface is sufficiently strong, the larger the fiber aspect ratio the better the stress transfer and the better the overall composite properties up to a critical length[39-41]. Our observation of a fluorescence slope increase with increased tQD concentration is similar. As the filler concentration increases, the average aggregate size increases and the spacing between aggregates decreases, analogous to a larger aspect ratio in ceramic fiber-polymer composites. This augmented interaction between aggregates leads to a greater stress transfer to the tetrapod phase of the composite. A similar

result was recently reported with micrometer-sized ZnO tetrapods, though in that case a clear distinction between elastic and plastic regimes and good resemblance between tensile and fluorescence curve shapes

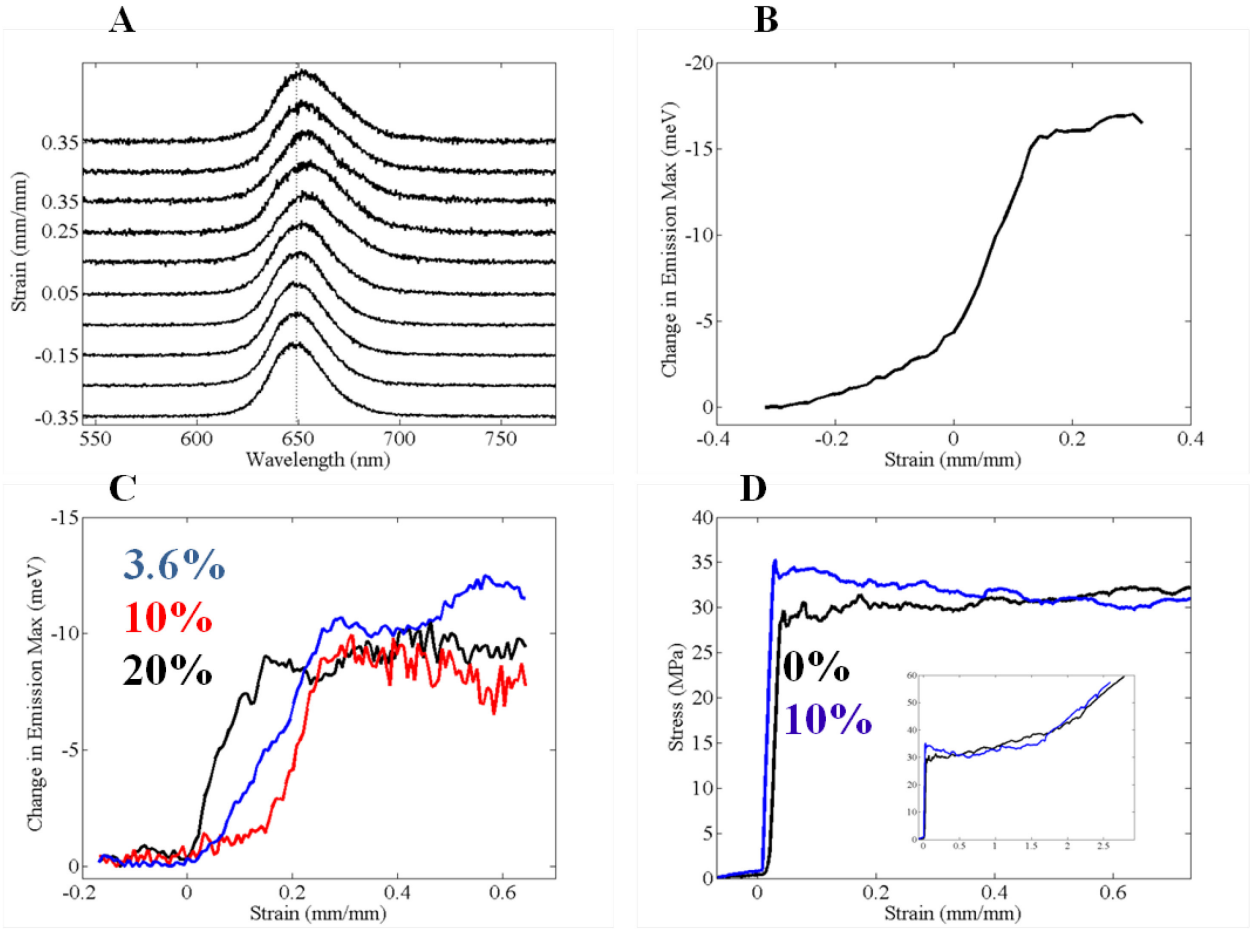


Figure 2.4: Comparison of tetrapod stress or strain gauge with commercial mechanical tensile testing machine (Agilent T150). (A) Selection of 10 raw spectra from a trial illustrating redshift of fluorescence emission as function of continuously imposed strain. (B) Fluorescence tensile curve obtained by fitting and plotting sequentially full set (approximately 200 spectra) of data represented in part A. Negative strain indicates slack. (C) Illustration of typical fluorescence tensile curves at three tetrapod loadings (3.6%, 10% and 20%), showing increase in slope of linear region as function of loading. The 10% curve is offset by 0.2 strain for clarity. (D) Comparative typical macroscopic uniaxial tensile curve on same batch of fibers (0% tetrapods and 10%).

was only seen at high (50% by weight) ZnO tetrapod concentrations[28]. In contrast, we see clear a distinction between elasticity and plasticity and an optical response approaching that in the mechanical tests at tQD concentrations as low as 3.6% by weight of the polymer. Additionally, in the work with ZnO tetrapods, oscillations were seen in the fluorescence tests at low tetrapod concentrations. This was attributed to non-interactive tetrapod domains in the polymer matrix[28]. In our case, we find oscillation-free behavior at even the lowest tQD concentrations in the polymer, meaning that interlocking is not necessary to achieve curves with relatively low noise and reasonable accuracy.

A complementary explanation for the particle concentration dependence is that aggregates near the fiber surface experience increased local strain due to the Poisson effect. PLLA has a Poisson's ratio of 0.4 indicating that it contracts roughly one unit radially for every two units extended axially[42]. Studies indicate that the Poisson's ratio is larger near the surface of a fiber[43]. Thus, this contracting force will be greatest at the surface. As the aggregate concentration increases, the number of aggregates proximal to the outer surface of the fiber does as well. Consequently, more aggregates are present in the region of maximum contracting force near the surface, leading to larger stress transfer and thus better response of the tQD probe. This explanation is consistent with the fact that the average maximum fluorescence peak shift also was seen to increase with concentration from −9.5 meV to −11.3 meV for 3.6% to 20% tQD concentrations by weight in the polymer, respectively, indicating that the sensor becomes more sensitive with increasing concentration of particles.

2.3.3 Incomplete Stress Transfer to the Nanoparticle Phase

It is apparent from parts B and D of Figure 2.4 that the linear elastic region as measured by the tQD sensor is much broader and covers more strain (6–30% extension) than the linear elastic region as measured by the UTM (which covers between 1 and 3%). This is likely due to poor stress transfer to the tQD filler. In the case of strong stress transfer, we would expect fluorescence shifts to occur over the same range of strain as seen in the mechanical data as well as significant mechanical property changes in the nanocomposite. The poor stress transfer is due to a weak interface between the nanocrystal and the polymer. The PLLA polymer is a hydrophilic aliphatic polyester with hydrogen bonding between the chains. The tQDs, with their native hydrophobic ligands, cannot participate in the hydrogen bonding. This unfavorable ligand-polymer interaction leads to the observed tQD clusters in the polymer matrix (Figure 2.3B and C). Prior demonstrations of the tQD support the idea of partial stress transfer to the particle. Previously, tQDs were added to hydrophilic polymers, such as Nomex, through diffusion after application of a droplet of particle solution. Diffusion likely creates a weaker particle–polymer interface than electrospinning and explains why a smaller maximum particle shift was seen in previous work[29]. This suggests the tQD could also be used to optically probe the particle–polymer interface strength in composite materials. Future studies to use the tQD as a probe of the relationship between stress transfer and particle-polymer interface are proposed at the end of this chapter.

Despite the incomplete stress transfer to the particle phase, the tetrapod fluorescence still clearly responds to fiber deformation. This demonstrates the tQD's usefulness in reporting phase-specific mechanical information in composite materials. The UTM load cell senses the macroscopic strain, while the tQD is only sensitive to nanoscale deformations that introduce a strain in the CdSe/CdS nanocrystal lattice. These latter deformations may arise from nanoscale particle–particle interactions (inter- and intra-aggregate interactions) or direct nanoscale particle–polymer interaction, but not from purely polymer molecular modes of deformation such as amorphous twist-tie chain unraveling, backbone covalent bond stretching, and others discussed above[44]. The phase-specific probing behavior of the tQD helps explain the differences between the optical and mechanical testing shown in Figure 2.4.

2.3.4 Stress Relaxation

In service, parts often undergo more complex stress-states than pure tensile elongation, such as compression, torsion, stress relaxation and hysteresis. For example, heavy materials are often held together by an epoxy, which might undergo relaxation over time. These more complex behaviors are of key importance to understanding polymer dynamics. Furthermore, the ability to monitor relaxation in real time could be used to predict and study failure of components. Therefore, with an eye toward applications and advanced fundamental studies, we also examined stress relaxation and hysteresis in the nanocomposite, both optically and mechanically.

To the best of our knowledge, this has never been mapped using self-sensing nanoscale sensors embedded into a material. Figure 2.5A depicts the results of a mechanical tensile test in which a fiber containing 10% tetrapods by weight was stretched to 77% strain and held there for approximately 53 seconds. Stress is plotted as a function of time and shows an exponential falloff associated with stress relaxation in the polymer[45]. Figure 2.5B illustrates a fluorescence test performed under identical strain rate and holding conditions as the mechanical test. The same distinct exponential falloff in stress relaxation is seen. The stress relaxation tests in the UTM were performed on 5 fibers of each tQD concentration (15 fibers total) and no difference in load relaxation properties was observed as a function of concentration. The mechanical stress relaxation behavior showed a 28.8 ± 0.8% 30.2 ± 0.7%, and 29.9 ± 1.38% relaxation for fibers containing 3.6%, 10%, and 20% tetrapods by weight, respectively. The average over all 15 samples was 29.6 ± 1.13% relaxation. By contrast, the average over 45 fiber samples of stress relaxation measured optically was 20.9 ± 6.24% relaxation. Given that the mechanical test measures macroscale stress relaxation while the tetrapod sensing of stress relaxation originates from multiple dispersed local nanoscale polymer deformations, the degree of agreement between the two measurements is striking and demonstrates that the tetrapod can be an effective nanoscale sensor for stress relaxation, in addition to tensile properties. This may be useful for a variety of applications as it demonstrates an optical means of determining stress relaxation prior to failure in structural materials. Effects of the filler probe on mechanical properties of the composite are addressed in section 2.5. We observed a faster mechanical stress relaxation rate, (see Appendix figure A1.1, for exponential decay fits) consistent with the incomplete stress transfer to the tetrapod filler phase. In the case of the nanotetrapod–PLLA polymer nanocomposite, the load sensor is the filler phase and therefore only measures a fraction of the load felt by the polymer matrix. The smaller exponential stress falloff measured optically is thus in accord with the broadness of the linear response of the tQD as compared to that measured by the tensile testing machine.

2.3.5 Cyclic Deformation

We also used the tQD as a probe for sensing the response of the single PLLA fibers to cyclic loading, again as compared to mechanical tests, and found telling differences between the hysteresis curves obtained via the two methods. Figure 2.6A shows a hysteresis loop done on a 10% tetrapod–PLLA composite fiber measured mechanically. The fiber was stretched to approximately 10% strain and returned to zero strain at the same strain rate. As before, the same strain rates and test conditions were used with both sets of tests. The fiber shows clear hysteresis in the first cycle of the mechanical test, but does not show hysteresis in the first optical test cycle

(Fig. 2.6B). If taken as a sensor of the polymer matrix, the tetrapod is reporting that some of the polymer plastic deformation is elastic. We believe that this again indicates that the tQD sensor is, in the PLLA nanocomposite system, reporting the stress that is transferred to the particle phase rather than the stress felt by the matrix. Furthermore, the fluorescence shift is based on an elastic deformation of the tQD crystal lattice[46,47] and is not expected to show hysteresis[48]. The complete recovery of the initial width and position of the fluorescence signal also indicates the lack of residual stress in the tetrapod. Possibly, the poor particle–polymer interface, and the accompanying aggregation, may limit stress transfer to the tetrapods and prevent permanent deformation of the crystal lattice of a filler particle.

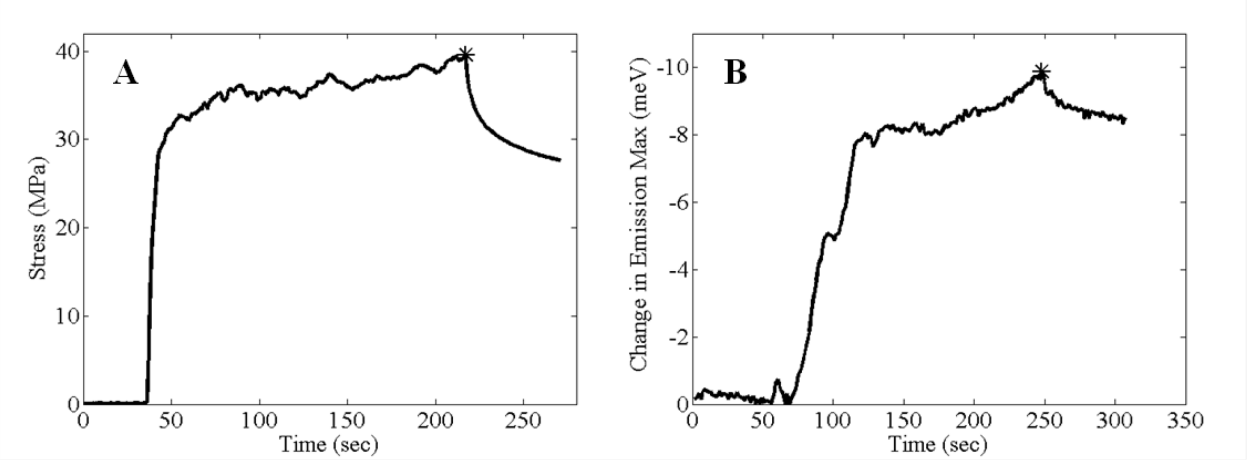


Figure 2.5: Comparison of load relaxation behavior between tetrapod probe and commercial tensile tester. (A) Macroscopic mechanical test data illustrating load relaxation. (B) Fluorescence test data obtained under same mechanical test conditions (strain rate, percent extension, and load relaxation time) illustrating load relaxation. * indicates when strain was held at 77%.

Parts C and D of Figure 2.6 represent the trials shown in Parts A and B, respectively, only now as a function of time. In these plots, the clear resemblance between the latter cycles is shown, whereas the first cycle again displays plastic deformation. Figure 2.6D also illustrates a level of baseline optical noise present in between optical test cycles. The noise is due to the fiber coming out of focus between cycles. Upon plastic deformation, the fiber length increases, and so upon returning to zero strain between cycles, it goes out of focus.

As the cyclic deformation has nearly no hysteresis in the tetrapod fluorescence shift, no energy is dissipated in the tetrapods even when a great deal is lost in the polymer; this is evident through the degree of plastic deformation present in the mechanical hysteresis curves.

These observations of hysteresis imply that in composites characterized by weak nanofiller-polymer interfaces, such as the nanocomposite material presented here, failure occurs due to void formation in the polymer matrix or around the particle–polymer interface rather than within the tetrapod nanoparticle phase. Through hysteresis data, the tQD therefore provides a simple imaging technique for determining the source of failure in a nanocomposite.

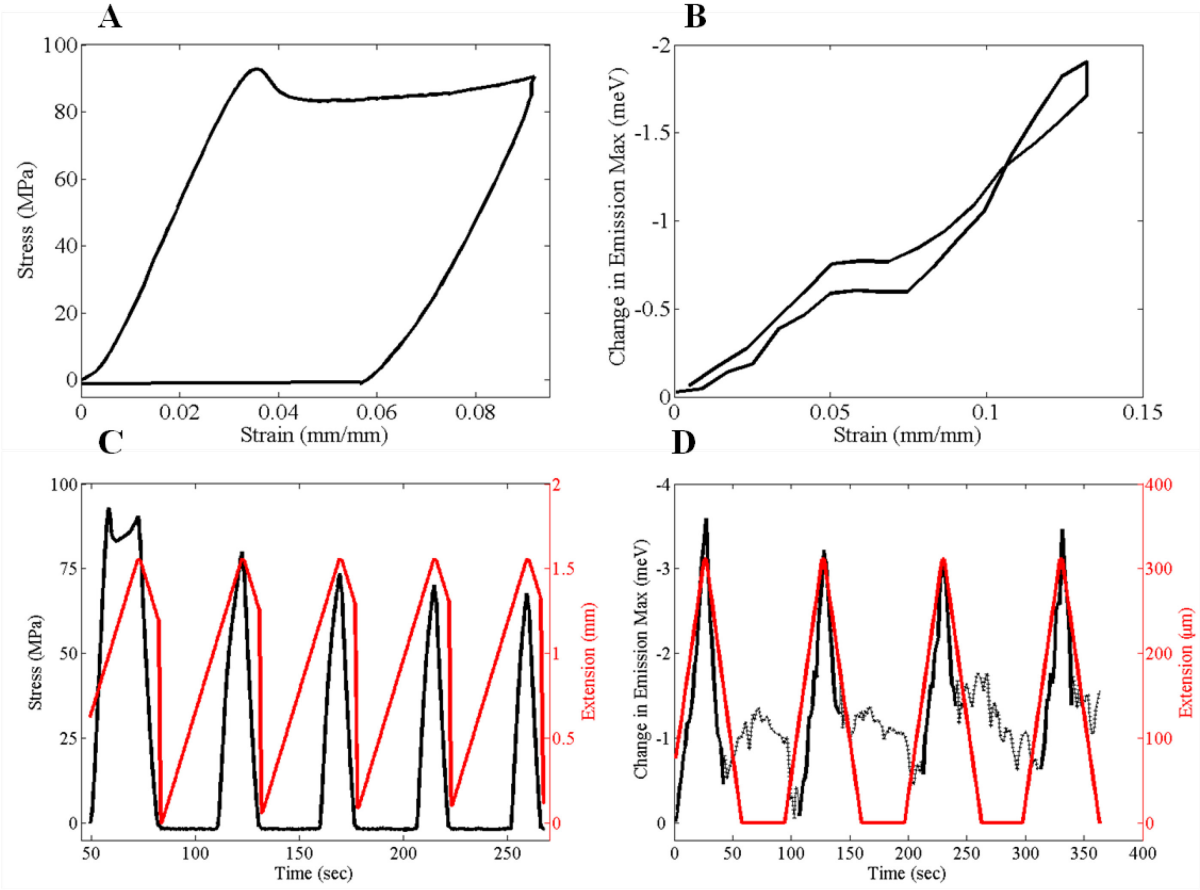


Figure 2.6: Comparison of hysteresis behavior between the macroscopic mechanical test and tQD probe. (A) Mechanical hysteresis loop illustrating plastic deformation and accompanying energy loss. (B) Fluorescence 'hysteresis' curve obtained under same mechanical test conditions (strain rate, percent extension, and return rate) illustrating little to no hysteresis. (C) Hysteresis loops from trials shown in part A plotted versus time. (D) Fluorescence 'hysteresis' loops of data from trials in plot B plotted versus time. Dashed regions indicate periods where fiber was not in focus due to slack from plastic deformation.

2.4 Demonstration of Versatility and Robustness

In order to demonstrate that the tQD's previously reported use as an internal stress sensor is robust and versatile, we tested electrospun nanoparticle-polymer composites of varying structure. The additional polymers tested in this study are Kraton G (styrene–ethylene/butylenes–styrene, aka SEBS), polycaprolactone (PCL), and polybutadiene (PBD). Previous work from this group has used nylon, polyester, Nomex, and polylactic acid (PLLA). Table 2.1 includes molecular structures and selected physical properties to illustrate the major differences in these polymers.

These systems represent a wide range of polymer properties, varying from hydrophilic (PCL and PLLA) to hyodrophobic (SEBS), semi-crystalline (PLLA) to entirely amorphous (SEBS and PBD), and fairly compliant (SEBS, E ~ 40 MPa) to very stiff (Nomex, E ~ 20 GPa). Additionally, thin-film composites of SEBS were prepared by simply drying mixed solutions of nanoparticles

and SEBS in chloroform using a gentle stream of air. Remarkably, in every case the unmodified embedded tQD fluorescence shifts with applied strain.

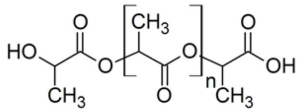
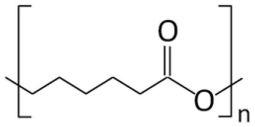
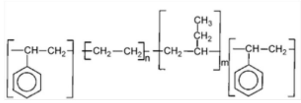
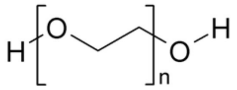
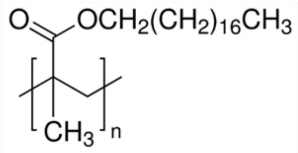
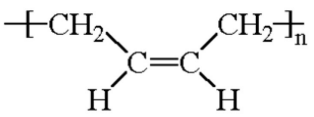
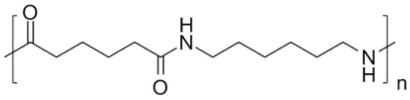
Polymer	Structure	Young's Modulus	Demonstrate Processing Methods
PLLA		1-3 GPa	Electrospun fibers
PCL		0.1-0.5 GPa	Electrospun fibers
Kraton G (SEBS)		20-140 MPa	Electrospun fibers and film solutions
PEO		0.5-1 GPa	Electrospun fibers
PODMA		-	Electrospun fibers
PBD		-	Electrospun fibers
Nylon		5-4 GPa	Diffusion from pippeting

Table 2.1: The tQD has proven to be compatible with a variety of polymer structures and processing techniques.

Side by side optical and mechanical tests of electrospun fibers were again performed in order to compare the fluorescence response of the tQD smart composite with traditional tensile testing results (Fig. 2.7). In contrast to previous tests in PLLA composite fibers, in SEBS stress is transferred immediately to the tetrapods and continuously throughout extension as evidenced by the fluorescence shift. In PLLA composites, the tQD-polymer interface was relatively weak due to the hydrophobic nature of the tQD ligands and the hydrophilic nature of PLLA. In the case of SEBS, it is expected that the composite has a stronger interface due to the like-like interactions of the tQD ligands with the ethylene/butylenes section of the polymer structure.

Additionally, the particles can only report stresses transferred to their domain, which in the case of PLLA is the relatively compliant region of the semi-crystalline polymer structure. As illustrated in Figure 2.2, a semicrystalline polymer has many deformation pathways that would not transfer stress through the amorphous region of the material where the tQD is located. Since SEBS is an entirely amorphous elastomer, any microscale deformation mechanism involves some stress transfer to the nanoparticle phase. The comparison of mechanical and optical data in Figure 2.7 demonstrates that is the case.

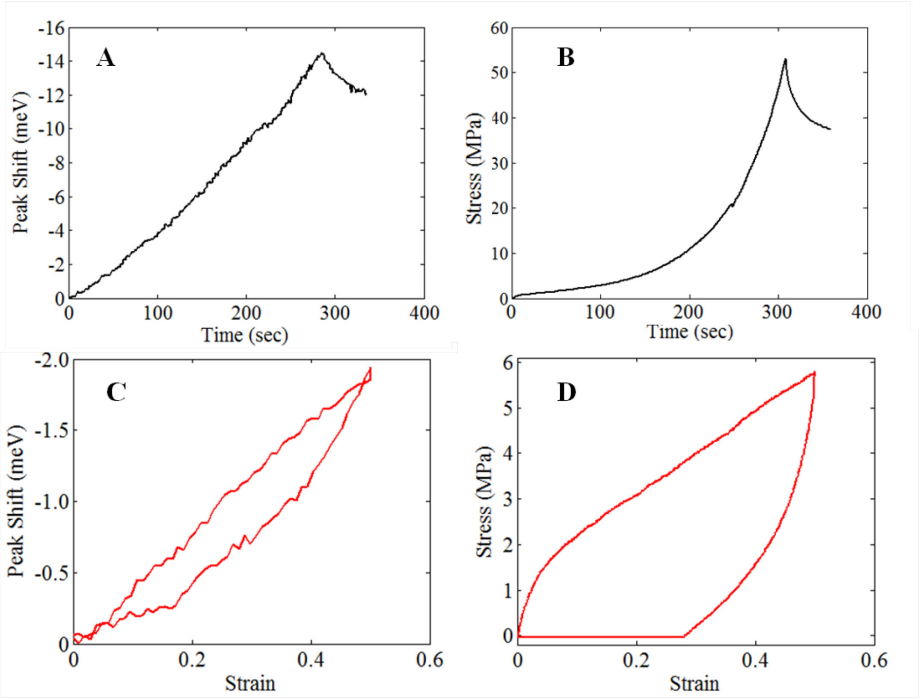


Figure 1.7: Optical (A and C) and mechanical (B and D) characterization of SEBS-tQD composites. (A and B) represent tensile extensions and stress relaxation performed under identical conditions to Figure 2.4 for optical and mechanical measurements, respectively. (C and D) illustrate hysteresis curve for optical and mechanical tests, respectively.

In comparative studies across polymer structures, it is important to remember that the fluorescence peak will only shift in response to forces transferred across the polymer-particle interface that are strong enough to deform the crystal lattice of the CdSe/CdSe nanoparticle. The fluorescence shift only occurs when a deformation mechanism induces a strain in the particle. All other deformation mechanisms involving only the polymer phase do not result in a optical response. These results show that in contrast to PLLA composites, the SEBS composites continuously deform the filler particle. This insight is unique to the tQD sensor and should be considered in development of nanoparticle-polymer composites.

Finally, these studies also indicate that the tQD is fairly indifferent to composite processing technique. Indirect diffusion into polymer fibers via pipetting[37], electrospinning to form fiber composites[49], and solution deposition to form films all result in functional composites. This also highlights that the tQD can be used to investigate the internal strain states of many polymer systems with essentially no modifications.

2.5 Effects on Composite Mechanical Properties

Tetrapod probes also offer the ability to enhance the mechanical properties of their host material beyond unbranched nanoparticles such as quantum dots and nanorods. However, the effects of adding a nanoparticle filler into a polymer can vary from markedly from one polymer to another. For example, the modulus of PLLA-tetrapod composites did not differ significantly from pure PLLA. In contrast, SEBS-tetrapod composites were stiffer than pure SEBS and SEBS-nanoparticle composites of nanorods and quantum dots. The following discussion explains these two differing results.

Mechanical tests performed on the tensile testing machine on a total of over 70 PLLA fibers, found no significant trend in modulus (measured by taking the slope of the initial linear elastic region of the engineering stress–strain curve), toughness (measured by taking the area under the curve of the entire engineering stress–strain curve), or stress and strain at failure with concentration increased from 0% to 20% by weight of tetrapods in the PLLA polymer. Even at 40%, there is no significant change in elastic modulus although there is a decrease in toughness and other mechanical properties, despite bulk CdS and electrospun PLLA having Young's moduli of approximately 50 GPa and 2 GPa, respectively (Appendix, Table A1.2). This is unusual as many composite systems of semiconductor quantum dots[50-52], micrometer-scale tetrapods[28], and other polymer–ceramic systems show modulus increases with such weight percent additions[53], sometimes accompanied by decreases in failure strains and toughness. Although opposite effects have also been observed[9], it is perhaps surprising that all the tensile mechanical properties remain relatively unchanged with such high concentration of tetrapods. However, we believe that this is due to the combination of the weak tQD–polymer interface and PLLA structural variations caused by electrospinning. The poor stress transfer due to the weak interface explains why the measured Young's moduli do not follow a straightforward "rule of mixtures" analysis[53]. Regarding structural variations, PLLA is a semicrystalline polymer with multiple phases determining its mechanical properties. These phases can clearly be observed as darker and lighter (crystalline and amorphous) regions in our TEM images. Small changes in the processing of the electrospinning precursor solutions, such as those introduced by large particle loading, may impact the crystallinity of the resultant fibers. Collection conditions as well as inherent electric field variations across the dual-rod electrodes may also result in structural variations. Accordingly, dynamic scanning calorimetry (DSC) analysis showed significant variation in crystallinity and grain size across samples, but no net effects on the crystallinity and polymer structural and thermal properties as a function of tQD concentration in the nanocomposite. The result is a material that shows little change in a wide range of mechanical properties even at large particle volume fractions.

SEBS composites provide a contrasting case, which is unsurprising given the previously discuss evidence for a more strongly bound nanoparticle in these materials. Tensile tests to failure provided a mean composite modulus for tQD and nanorod composites of 5%, 10%, and 20% by weight (corresponding to 1.25%, 2.5%, and 5% by volume) was found (Appendix, Figure 1.2). It is immediately apparent that tQDs enhance the fiber's modulus to a greater extent than nanorods do. This is despite the fact that both types of particles are made of CdSe/CdS, are present in the same volume percent, and are interfaced with the polymer via the same like-like interactions.

The reason for the added enhancement in tQD composites is that branched nanoparticles on the size scale of this study are best considered as randomly oriented chopped fiber-like composites. Though carbon fiber composites, and microneedle composites are typically considered as fiber-composite systems, to the best of our knowledge a quantum dot-composite has never been demonstrated to behave in a fiber-like manner[54-56]. In an ideal fiber composite, fillers aligned with the tensile strain result in an overall modulus defined by the rule of the mixtures; whereas, fibers that are orthogonal result in a modulus defined by the inverse rule of mixtures. In the case of the filler particle being much stiffer than the surround matrix, an aligned composite should be much stiffer than the orthogonal case.

The composites in this work are comprised of randomly aligned particle aggregates. However, due to its three-dimensionally symmetric branched structure, a single tQD is much more likely to be partially aligned with a strain tensor than a cylindrical nanorod. In essence, nanorods are anisotropic whereas tetrapods are isotropic in the randomly oriented composites studied here. This means that nanorods can take extremely different orientations with respect to the stretching axis (parallel or perpendicular to it), while tetrapods cannot. This experimentally observed dependence on isotropy can be rationalized by the fact that the nanorod elastic modulus differs along the two different axes of loading. Hence, the effective elastic modulus along the axis of loading is a weighted average of the two elastic moduli according to the orientation from the axis of loading. As the nanoparticle becomes more isotropic while maintaining fiber-like characteristic, such as a tetrapod, this dependence on orientation diminishes as the elastic moduli along the orthogonal axes converges to a single value.

2.6 Conclusions and Future Studies

These experiments build upon the foundation of the tetrapod as not only an optical strain gauge, but as a tool for investigating nanoscale mechanisms of deformation and stress transfer across phases of complex composite materials. The tQD has now been shown to be a highly versatile sensor even without exploiting its easily accessible surface chemistry. Further tailoring the polymer-particle interface through ligand exchange on the nanoparticle will allow for more in depth studies of stress transfer. Already, we have seen that surprising result that the interfaces in SEBS-tQD composites and PLLA-tQD composites result in shifts of similar magnitude despite being of a chemically very different nature. Whether this is due to the relatively weak binding forces involved in both cases or to some inherent limit on stress transfer in these types of composites has yet to be seen.

In order to more deeply understand the fluorescence response, we also must have a more thorough understanding of the effects of orientation, sheer, normal, compressive, and mixed forces on the electronic structure of the tetrapod. The current assumption of a simple uniaxial deformation has proven to be useful, but there are clearly more levels of complexity accessible through these types of experiments.

Chapter 2 References:

1. Balazs, A.; Emrick, T.; Russell, T., Nanoparticle Polymer Composites: Where Two Small Worlds Meet. *Science* 2006, 314, 1107-1110.
2. Resch-Genger, U.; Grabolle, M.; Cavaliere-Jaricot, S.; Nitschke, R.; Nann, T., Quantum dots versus organic dyes as fluorescent labels. *Nat Meth* 2008, 5, 763-775.
3. Black, A. L.; Lenhardt, J. M.; Craig, S. L., From molecular mechanochemistry to stress-responsive materials. *Journal of Materials Chemistry* 2011, 21, 1655-1663.
4. Callister, W. D.; Rethwisch, D. G., *Materials Science and Engineering: An Introduction*. John Wiley & Sons Canada, Limited: 2009.
5. Papakonstantopoulos, G. J.; Riggleman, R. A.; Barrat, J.-L.; de Pablo, J. J., Molecular plasticity of polymeric glasses in the elastic regime. *Physical Review E* 2008, 77, 041502.
6. Patlazhan, S.; Remond, Y., Structural mechanics of semicrystalline polymers prior to the yield point: a review. *Journal of Materials Science* 2012, 47, 6749-6767.
7. Thomas, C.; Ferreiro, V.; Coulon, G.; Seguela, R., In situ AFM investigation of crazing in polybutene spherulites under tensile drawing. *Polymer* 2007, 48, 6041-6048.
8. Auras, R. A.; Lim, L.-T.; Selke, S. E. M.; Tsuji, H., *Poly (lactic acid): synthesis, structures, properties, processing, and applications*. John Wiley & Sons: 2011; Vol. 10.
9. Drumright, R. E.; Gruber, P. R.; Henton, D. E., Polylactic acid technology.*Advanced materials* 2000, 12, 1841-1846.
10. Giordano, R. A.; Wu, B. M.; Borland, S. W.; Cima, L. G.; Sachs, E. M.; Cima, M. J., Mechanical properties of dense polylactic acid structures fabricated by three dimensional printing. *Journal of Biomaterials Science, Polymer Edition*1997, 8, 63-75.
11. Kenawy, E.-R.; Bowlin, G. L.; Mansfield, K.; Layman, J.; Simpson, D. G.; Sanders, E. H.; Wnek, G. E., Release of tetracycline hydrochloride from electrospun poly (ethylene-co-vinylacetate), poly (lactic acid), and a blend.*Journal of controlled release* 2002, 81, 57-64.
12. Badami, A. S.; Kreke, M. R.; Thompson, M. S.; Riffle, J. S.; Goldstein, A. S., Effect of fiber diameter on spreading, proliferation, and differentiation of osteoblastic cells on electrospun poly (lactic acid) substrates. *Biomaterials* 2006, 27, 596-606.
13. Greiner, A.; Wendorff, J. H., Electrospinning: a fascinating method for the preparation of ultrathin fibers. *Angewandte Chemie International Edition* 2007, 46, 5670-5703.
14. Gupta, B.; Revagade, N.; Hilborn, J., Poly (lactic acid) fiber: an overview.*Progress in polymer science* 2007, 32, 455-482.
15. Huang, Z.-M.; Zhang, Y. Z.; Kotaki, M.; Ramakrishna, S., A review on polymer nanofibers by electrospinning and their applications in nanocomposites.*Composites science and technology* 2003, 63, 2223-2253.
16. Odian, G., *Principles of Polymerization*. Wiley: 2004.
17. Ciprari, D.; Jacob, K.; Tannenbaum, R., Characterization of Polymer Nanocomposite Interphase and Its Impact on Mechanical Properties. *Macromolecules* 2006, 39, 6565-6573.
18. Schadler, L. S.; Giannaris, S. C.; Ajayan, P. M., Load transfer in carbon nanotube epoxy composites. *Applied Physics Letters* 1998, 73, 3842-3844.
19. Velasco-Santos, C.; Martinez-Hernandez, A. L.; Castano, V. M., Carbon nanotube-polymer nanocomposites: The role of interfaces. *Composite Interfaces* 2005, 11, 567-586.
20. Ingrid De, W., Micro-Raman spectroscopy to study local mechanical stress in silicon

integrated circuits. *Semiconductor Science and Technology* 1996, 11, 139.
21. Sicardy, O.; Touet, I.; Rieutord, F.; Eymery, J., Stress Measurements in Thin Zirconia Films At 300°C Using Synchrotron Radiation. *Journal of Neutron Research* 2001, 9, 263-272.
22. Vaudin, M. D.; Gerbig, Y. B.; Stranick, S. J.; Cook, R. F., Comparison of nanoscale measurements of strain and stress using electron back scattered diffraction and confocal Raman microscopy. *Applied Physics Letters* 2008, 93, -.
23. Rabe, U.; Janser, K.; Arnold, W., Vibrations of free and surface-coupled atomic force microscope cantilevers: Theory and experiment. *Review of Scientific Instruments* 1996, 67, 3281-3293.
24. Yamanaka, K.; Nakano, S., Ultrasonic atomic force microscope with overtone excitation of cantilever. *Japanese journal of applied physics* 1996, 35, 3787-3792.
25. Odegard, G. M.; Gates, T. S.; Herring, H. M., Characterization of viscoelastic properties of polymeric materials through nanoindentation. *Experimental Mechanics* 2005, 45, 130-136.
26. Liang, X.; Oldenburg, A. L.; Crecea, V.; Chaney, E. J.; Boppart, S. A., Optical micro-scale mapping of dynamic biomechanical tissue properties. *Optics Express* 2008, 16, 11052-11065.
27. Kamat, N. P.; Liao, Z.; Moses, L. E.; Rawson, J.; Therien, M. J.; Dmochowski, I. J.; Hammer, D. A., Sensing membrane stress with near IR-emissive porphyrins. *Proceedings of the National Academy of Sciences* 2011, 108, 13984-13989.
28. Jin, X.; Götz, M.; Wille, S.; Mishra, Y. K.; Adelung, R.; Zollfrank, C., A Novel Concept for Self-Reporting Materials: Stress Sensitive Photoluminescence in ZnO Tetrapod Filled Elastomers. *Advanced Materials* 2013, 25, 1342-1347.
29. Stevenson, A.; Jones, A.; Raghavan, S., Stress-Sensing Nanomaterial Calibrated with Photostimulated Luminescence Emission. *Nano Letters* 2011, 11, 3274-3278.
30. Stone, J. W.; Sisco, P. N.; Goldsmith, E. C.; Baxter, S. C.; Murphy, C. J., Using Gold Nanorods to Probe Cell-Induced Collagen Deformation. *Nano Letters* 2006, 7, 116-119.
31. Kolle, M.; Lethbridge, A.; Kreysing, M.; Baumberg, J. J.; Aizenberg, J.; Vukusic, P., Bio-Inspired Band-Gap Tunable Elastic Optical Multilayer Fibers. *Advanced Materials* 2013, 25, 2239-2245.
32. Taylor, G., Disintegration of water drops in an electric field. *Proceedings of the Royal Society of London. Series A. Mathematical and Physical Sciences* 1964, 280, 383-397.
33. Behler, K. D.; Stravato, A.; Mochalin, V.; Korneva, G.; Yushin, G.; Gogotsi, Y., Nanodiamond-Polymer Composite Fibers and Coatings. *ACS Nano* 2009, 3, 363-369.
34. Ko, F.; Gogotsi, Y.; Ali, A.; Naguib, N.; Ye, H.; Yang, G. L.; Li, C.; Willis, P., Electrospinning of Continuous Carbon Nanotube-Filled Nanofiber Yarns. *Advanced Materials* 2003, 15, 1161-1165.
35. d'Almeida, J. R. M.; Monteiro, S. N.; Menezes, G. W.; Rodriguez, R. J. S., Diamond-Epoxy Composites. *Journal of Reinforced Plastics and Composites* 2007, 26, 321-330.
36. Jin, S. H.; Park, Y.-B.; Yoon, K. H., Rheological and mechanical properties of surface modified multi-walled carbon nanotube-filled PET composite. *Composites Science and Technology* 2007, 67, 3434-3441.
37. Choi, C. L.; Koski, K. J.; Sivasankar, S.; Alivisatos, A. P., Strain-Dependent Photoluminescence Behavior of CdSe/CdS Nanocrystals with Spherical, Linear, and Branched Topologies. *Nano Letters* 2009, 9, 3544-3549.

38. Choi, C. L.; Koski, K. J.; Olson, A. C. K.; Alivisatos, A. P., Luminescent nanocrystal stress gauge. *Proceedings of the National Academy of Sciences* 2010, 107, 21306-21310.
39. Lodha, P.; Netravali, A., Characterization of interfacial and mechanical properties of "green" composites with soy protein isolate and ramie fiber. *Journal of Materials Science* 2002, 37, 3657-3665.
40. Takagi, H.; Ichihara, Y., Effect of Fiber Length on Mechanical Properties of Green Composites Using a Starch-Based Resin and Short Bamboo Fibers. *JSME International Journal Series A Solid Mechanics and Material Engineering* 2004, 47, 551-555.
41. Monette, L.; Anderson, M. P.; Ling, S.; Grest, G. S., Effect of modulus and cohesive energy on critical fibre length in fibre-reinforced composites. *Journal of Materials Science* 1992, 27, 4393-4405.
42. Rezgui, F.; Swistek, M.; Hiver, J. M.; G'Sell, C.; Sadoun, T., Deformation and damage upon stretching of degradable polymers (PLA and PCL). *Polymer* 2005, 46, 7370-7385.
43. Elliott, D. M.; Narmoneva, D. A.; Setton, L. A., Direct Measurement of the Poisson's Ratio of Human Patella Cartilage in Tension. *Journal of Biomechanical Engineering* 2002, 124, 223-228.
44. Lee, J.-Y.; Zhang, Q.; Emrick, T.; Crosby, A. J., Nanoparticle Alignment and Repulsion during Failure of Glassy Polymer Nanocomposites. *Macromolecules* 2006, 39, 7392-7396.
45. Tobolsky, A. V., Stress Relaxation Studies of the Viscoelastic Properties of Polymers. *Journal of Applied Physics* 1956, 27, 673-685.
46. Schrier, J.; Lee, B.; Wang, L. W., Mechanical and electronic-structure properties of compressed CdSe tetrapod nanocrystals. *J Nanosci Nanotechnol* 2008, 8, 1994-8.
47. Liang, X.; Oldenburg, A. L.; Crecea, V.; Chaney, E. J.; Boppart, S. A., Optical micro-scale mapping of dynamic biomechanical tissue properties. *Optics Express* 2008, 16, 11052-11065.
48. Raja, S. N.; Olson, A. C. K.; Thorkelsson, K.; Luong, A. J.; Hsueh, L.; Chang, G.; Gludovatz, B.; Lin, L.; Xu, T.; Ritchie, R. O.; Alivisatos, A. P., Tetrapod Nanocrystals as Fluorescent Stress Probes of Electrospun Nanocomposites. *Nano Letters* 2013, 13, 3915-3922.
49. Mathur, V.; Dixit, M.; Rathore, K. S.; Saxena, N. S.; Sharma, K. B., Morphological and mechanical characterization of a PMMA/CdS nanocomposite. *Frontiers of Chemical Science and Engineering* 2011, 5, 258-263.
50. Kaur, H.; Banipal, T. S.; Thakur, S.; Bakshi, M. S.; Kaur, G.; Singh, N., Novel Biodegradable Films with Extraordinary Tensile Strength and Flexibility Provided by Nanoparticles. *ACS Sustainable Chemistry & Engineering* 2012, 1, 127-136.
51. Patidar, D.; Agrawal, S.; Saxena, N. S., Stress-strain Behavior of CdS/PMMA Nano-composite. In *Journal of Polymer Engineering*, 2010; Vol. 30, p 565.
52. Liu, H.; Webster, T. J., Mechanical properties of dispersed ceramic nanoparticles in polymer composites for orthopedic applications. *Int J Nanomedicine* 2010, 5, 299-313.
53. Marom, G.; Fischer, S.; Tuler, F. R.; Wagner, H. D., Hybrid effects in composites: conditions for positive or negative effects versus rule-of-mixtures behaviour. *Journal of Materials Science* 1978, 13, 1419-1426.
54. Frogley, M. D.; Ravich, D.; Wagner, H. D., Mechanical properties of carbon nanoparticle-reinforced elastomers. *Composites Science and Technology* 2003, 63, 1647-1654.

55. Kim, J.-s.; Reneker, D. H., Mechanical properties of composites using ultrafine electrospun fibers. *Polymer Composites* 1999, 20, 124-131.
56. Sawicka, K.; Gouma, P., Electrospun composite nanofibers for functional applications. *Journal of Nanoparticle Research* 2006, 8, 769-781.

Chapter 3: Tetrapods as Biological Sensors

3.1 Forces at the Cellular Level - Mechanoreciprocity.....26
3.2 Collagen and Tumorigenesis.....27
3.3 Tetrapods and Cellular Forces 29
3.3.1 Tetrapod-Collagen Composites 30
3.4 Future Studies 32
3.4.1 Molecular Restructuring of the ECM 32
3.4.2 Biologically Relevant Cell Force Measurements 34
References.....36

3.1 Forces at the Cellular Level - Mechanoreciprocity

Cell-generated forces play a central role in tumor growth and invasion. In this section, we propose to use tetrapod quantum dot (tQD) to investigate the role of physical forces and mechanical properties in biological fibers and during cellular processes such as contraction, migration and branching morphogenesis. This project will combine tQD force sensors with cancer biology, and allow study of cellular forces in physiological conditions, which will inform our quantitative understanding of how cancers interact mechanically with their environment in a different way than normal cells. Proof-of-concept experiments are first demonstrated and future studies and their importance are proposed.

Biomechanical forces play an important role in cellular processes including contraction, motility, and metastasis. Cells feel substrate rigidity through mechanoreceptors, which lead to the formation of focal adhesions, remodeling of the cytoskeleton, and changes in gene expression. Stiffness of the extracellular matrix (ECM) can alter cell differentiation, migration, and invasive potential[1-4]. Cells respond to these mechanical cues by exerting reciprocal forces through both cytoskeleton-dependent and independent processes termed mechanoreciprocity. While it is clear that cell traction forces are intrinsically linked with ECM mechanics and play a central role in tumorigenesis and metastasis, the molecular scale restructuring of collagen during these processes is poorly understood. The development of tQDs as a biological strain gauge will allow for the first quantitative dynamic stress profiles of microscale collagen restructuring by biologically relevant crosslinkers and tumorigenic cells.

The spatial and temporal information obtained from this type of stress profile is not accessible using the current techniques available for the measurement of cell forces. High-density two-dimensional arrays of elastomeric posts have been widely used to measure cellular forces during migration[5]. These measurements are based on deducing the magnitude of traction forces from measuring the bending of an elastomeric post with a known modulus. While these studies have provided insights into the magnitude of cellular forces and made correlated measurements with actin localization[6,7], they have limited spatial resolution due to pillar spacing (typically about 10 μm) and cannot be performed in real-time with simultaneous monitoring of biochemical events. Furthermore, pillar-based measurements inherently perturb cell biomechanics due to spatial distribution of binding sites on the pillars[8]. An alternative technique relies on tracking the displacement of embedded fluorescent beads during cell-induced substrate deformations[9]. However, both of these techniques are only capable of reporting local strains and assume mechanical homogeneity of the substrate[10]. While that assumption is reasonable for synthetic

polymer substrates, physiological substrates are mechanically inhomogenous and such techniques would be difficult to implement. A more recent advancement in cell traction measurements has been the use of FRET-based techniques[11]. These techniques have been used to probe the stretching of fibronectin and other cytoskeletal components during cell movement. However, they are only applicable to the piconewton (pN) force range and do not address the nanonewton (nN) forces to which tQDs are sensitive. Additionally, tQDs have the same advantage over FRET-based sensors as quantum dot labels do over any fluorescent molecule – quantum dots have broad absorbance, narrow emission, and do not easily photobleach.

Tetrapod quantum dots also offer improvement over techniques in acellular collagen measurements, which are similar to the previously discussed polymer probing techniques. Current biopolymer techniques are limited to studying the bulk mechanics of collagen gels under strain[12], require lengthy time scales for X-ray diffraction (XRD) and small angle X-ray scattering (SAXS) measurements of the microstructure[13], or must employ synchrotron radiation sources for fast microscale strain measurements[14]. We have built a custom tensile tester that is capable of making bulk mechanical measurements of collagen simultaneously with fluorescence monitoring of tQD signals. By using tQDs as our probe of microscale mechanics in collagen we can make stress profiles with approximately 1 μm^2 resolution at millisecond timescales.

Development of tQDs as biomechanical probes will enable investigations and promote the understanding of many force-dependent processes that are critical to tumor growth and metastasis. In the following proposed experiments, the microscale structure of collagen matrices under tensile strains will be spatially and temporally resolved for the first time. Real time restructuring of the collagen matrix with the addition of biologically relevant crosslinkers such as lysyl oxidase (LOX) and ribose will then be monitored and new stress profiles of collagen under tensile strain will be generated. Finally, the distribution of strain due to oxytocin-induced contractions of normal and tumor-derived myoepithelial cells will be investigated. These experiments will provide a quantitative molecular mechanical understanding of how collagen is restructured during tumor growth and how it differs from healthy cellular environments.

3.2 Collagen and Tumorigenesis

Collagen is the primary component of the ECM and exhibits a wide array of mechanical stability, strength, and stiffness depending on the specific tissue such as tendons, ligaments, skin, cornea, and bone in which it is found. The versatility of collagen is derived from modifications to its hierarchical structure. The basic building block of collagen is the tropocollagen molecule – a triple helix of approximately 280 nm in length and 1.5 nm in diameter comprised of three polypeptide helices[15] (Figure 3.1). The tropocollagen molecule can form higher level structures like fibrils and fibrils; however, the most relevant structure for our studies is the polymerized networks of tropocollagen molecules predominant in the ECM. Collagen has been a material of interest for some time due to its rigidly hierarchical structure spanning across the angrstrom, nanometer, and micrometer scales[16]. Despite being of great biological importance and one of the few hierarchical biological nanomaterials[17], the molecular deformation mechanisms of collagen under macroscale load are not well characterized or understood[15].

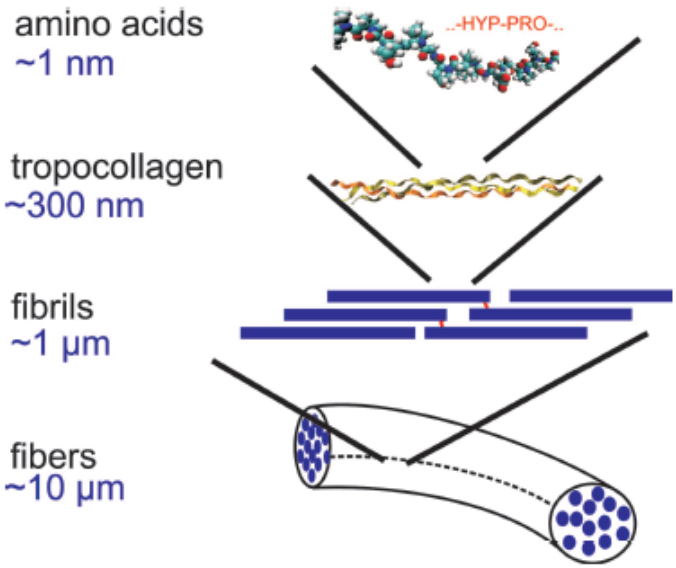


Figure 3.1: Collagen is remarkable for its highly structured composition at multiple levels. Three α-helices comprised typically of Gly-X-Y amino acids make up the triple helix of the tropocollagen molecule with proline and hydroxyproline being the most common X and Y constituent. These then form fibril bundles with regular D-spacing of approximately 67 nm. Higher order structures such as fibers, tendons, bone, and skin are possible depending on physiological conditions. Adapted from Reference 15.

Type I collagen is the most prevalent protein in mammals; however, we currently lack the ability to probe the mechanical heterogeneity of collagen. Presently, XRD and SAXS are the tools typically used for studying the molecular response to strain in collagen[17]. Both of these techniques rely on the ensemble measurement of a periodic structure over the size of the X-ray beam, which is typically on the order of hundreds of microns. Consequently, current techniques for probing collagen mechanics cannot be adapted to investigate microscale variations in response to the biologically relevant regime of forces. The tQD system will be the first to achieve a dynamic microscale map of the strain response of collagen. This quantitative understanding of the distribution of mechanical properties and how they change with strain is critical to understanding the interplay between cell and ECM during tumor growth and metastasis.

Tumor initiation has been shown to be accompanied by collagen crosslinking, which results in increased invasion[18]. Lysyl oxidase is secreted by tumorigenic cells to crosslink collagen and reduction of LOX impedes malignant progression. Again, current probes of collagen mechanics are incapable of mapping molecular changes to collagen mechanics during these crosslinking processes.

Tetrapod quantum dots will also shift investigations of cellular biomechanics towards probing stresses in more biologically relevant environments including more realistic matrix materials. Studies based on elastomeric posts require the substrate to be made of a patterned elastomeric polymer. As demonstrated in studies of synthetic polymers, the tQD can be incorporated into biological systems of any geometry, potentially leading to studies of forces from cells cultured in

three-dimensional environments. The tQD's optical response to stress can be easily monitored with spatial and dynamic resolution down to the capabilities of the best light microscope. Though not proposed in this study, tQDs have the potential to be the first probe of stresses generated by cells in a three-dimensional ECM with the ability to map the distribution of those forces throughout the ECM in real time.

3.3 Tetrapods and Cellular Forces

One of the major advantages of the tQD probe is its versatility and compatibility with a number of environments. It has also been shown to be responsive to several types of deformation tests – tensile, cyclic, and relaxation. This allows for the tQD as a biosensor to be demonstrated in a step-wise manner. First, the tQD was shown to respond to direct interactions from cardiomyocytes. Then, tQD-collagen composites were synthesized and tested for fluorescence response. The combination of these two results leads directly toward a method for measuring cellular forces and restructuring of the ECM in a more natural, three-dimensional environment.

Prior work performed jointly between the Alivisatos and Werb groups has also shown the suitability of the tQD for biological settings. In this study, cardiomyocytes were cultured directly on fibronectin-coated monolayers of tQDs (Fig. 3.2a). The contractile force due to cardiomyocyte beating was then measured using the resulting shifts in fluorescence from the tQDs (Fig 3.2B). To the best of our knowledge, this work represents the first example of a dynamic nanocrystal that can respond to cellular forces and demonstrates our probes sensitivity to cell-generated forces.

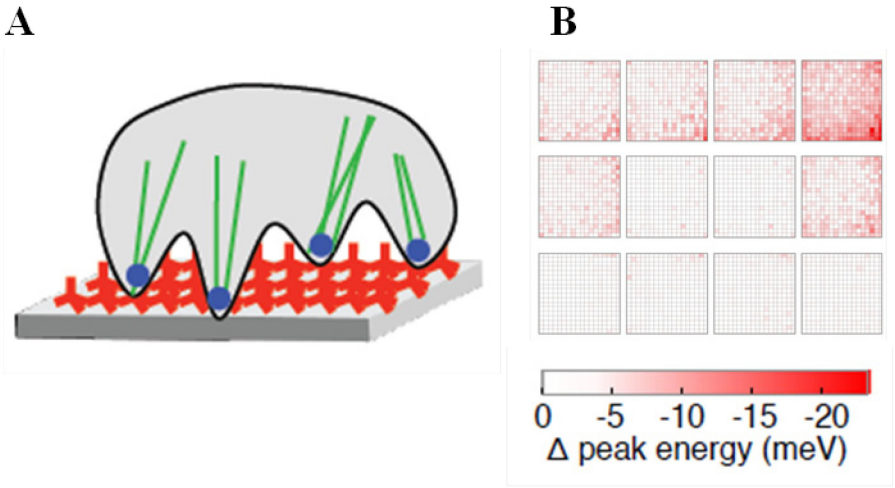


Figure 3.2: Schematic of a cell grown on a fibronectin-coated monolayer of tQDs. b) Spectral map snapshots of peak shifts from a cardiomyocyte-perturbed tQD array over time. The change in peak energy at each pixel is plotted relative to a standard spectral map containing the highest peak energies observed; each frame represents 350 ms spectral integration time. (I) and (II) are spectral snapshots taken on substrates with beating cardiomyocytes. (III) is an unchanging snapshot from a fibronectin-coated tQD grid with no cardiomyocytes. Side length is 40.7 µm.

3.3.1 Tetrapod-Collagen Composites

A complementary method of examining forces in mechanoreciprocity is to probe mechanical deformations in the ECM. This method through which the tQD is employed in analogous to the nanoparticle-polymer composites described in the previous chapter. Tetrapods can be embedded into a collagen matrix such that a deformation on the macroscale or distant from the tQD still produces some stress transfer to the nanoparticle and a resulting fluorescence shift.

In order to form collagen-tQD composites, bovine dermis type I collagen was polymerized and crosslinked following standard protocols[19]. The resultant gels were thick (approximately 1-2 cm) with Young's moduli on the order of 10-100 kPa. Tetrapods were incorporated into the gels via amide bound formation. Particles were first ligand-exchanged to poly(maleic anhydride-alt-1-tetradecene) (MAAT) through previously reported techniques[20]. The carboxylic acid group of the ligand and the primary amines native to the collagen peptide structure were reacted in the presence of N-hydroxysulfosuccinimide (NHS) and 1-ethyl-3-(3-dimethylaminopropyl) carbodiimide (EDC) in order to covalently link the tQD into the collagen structure. This protocol was adapted from Castaneda, et al.[21] who used it to covalently bind gold nanoparticles to tropocollagen.

The resulting composites were mechanically robust and easily transferred to a custom tensile tester which allowed for simultaneous optical and mechanical measurements (Fig. 3.3A and B). The homebuilt tensile tester was based off of a previously reported apparatus[22]. Briefly, a Mark-10 Series 5 force gauge was mounted across from a micrometer stage. A piece was cut out between the two sample clamps that was large enough to support a clear plastic buffer tray for collagen samples as an objective for optical measurements. The buffer tray also included a window made from a glass coverslip in order to avoid potential distortions through the plastic tray. These composites exhibited evenly dispersed particles (Fig. 3.3C) and stress-strain curves characteristic of collagen gels (Fig. 3.3D). However, they did not exhibit a fluorescence shift in response to tensile testing (Fig. 3.4).

Collagen is a biopolymer and has a repeating structure qualitatively similar to the synthetic polymers we have previously studied. Consequently, the microscale mechanisms of deformation – chain reorganization, backbone stretching, slipping, crack propagation, etc. – are categorically the same. However, the collagen fibers in this study are formed and tested as gels with embedded nanoparticles. Consequently, there is a much larger viscoelastic component to its stress-strain relationship. Water surrounding the collagen fibers flows during tensile testing. This kind of deformation is unlikely to result in much or any stress transfer to a nanoparticle. Of the variety of polymers composites tested and described in this manuscript, it is interesting to note that collagen is the only case in which no significant stress transfer could be observed.

In order to encourage larger stress transfer to the tQD, a higher level composite gel was synthesized. Essentially, we sought to create stress concentration in the vicinity of tQD by encumbering collagen chain movements. Collagen was again polymerized in the same manner, except PLLA-tQD electrospun fibers were included in the solution bath. Tangled mats of PLLA-tQD fibers (Fig 3.5A) were created by electrospinning onto an aluminum foil target suspended between the previously described collection rods. The gels composites were again crosslinked

via sulfo-NHS / EDC coupling in order to utilize the carboxylic acid groups present in the amorphous region of the PLLA structure.

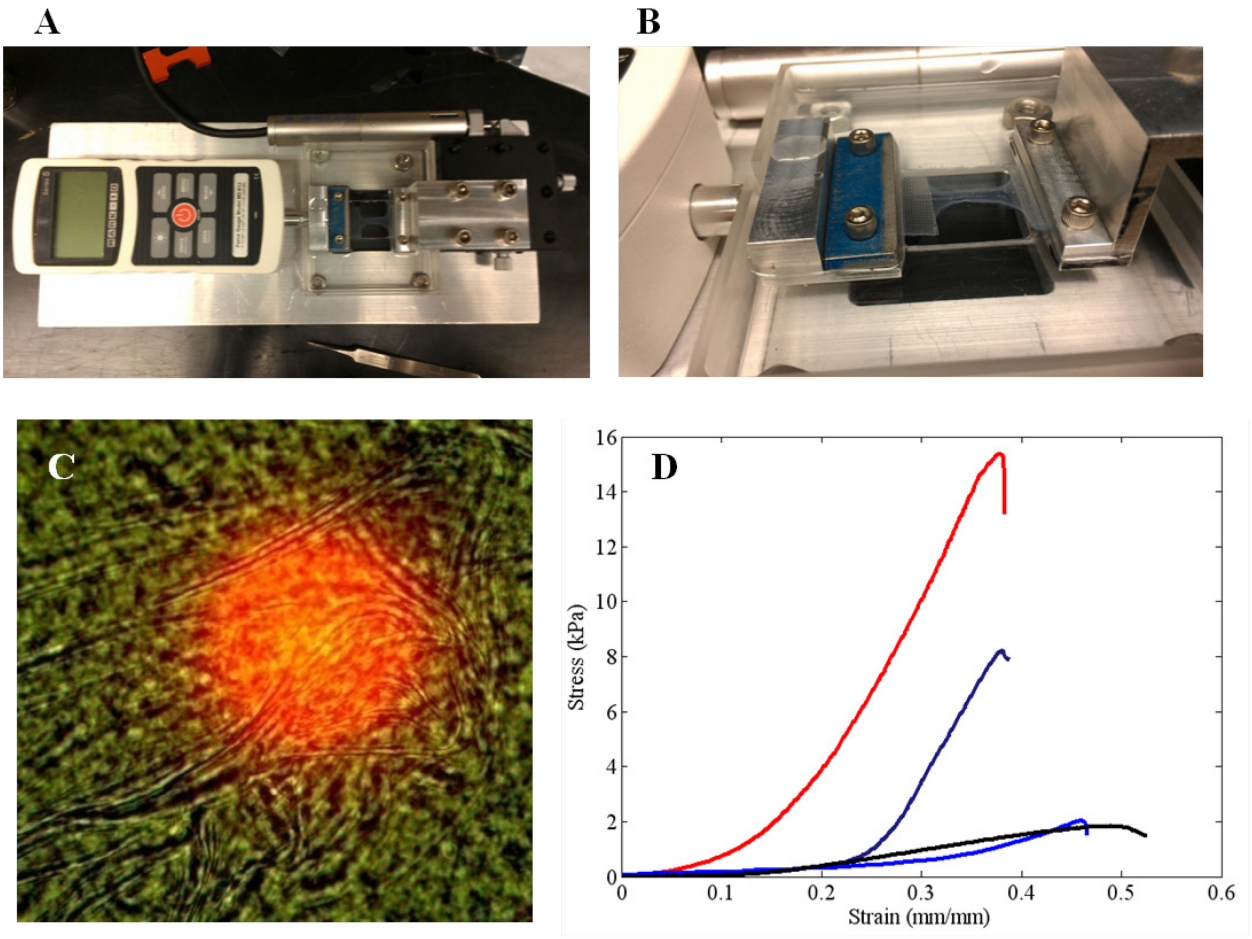


Figure 3.3: Characterization of collagen-tQD gels. (A) Custom build tensile tester for simultaneous optical and mechanical measurements of collagen films in buffer. (B) Example of mounted dog-bone collagen gel sample. (C) Emission of tetrapods (red circle) embedded in collagen gel (black and gold background) indicating even dispersion of particles in gel. (D) Mechanical testing of collagen gels without NHS-EDC induced crosslinking (black), after 1 hour of crosslinking (light blue), after 24 hours (dark blue) and with the inclusion of poly(MAAT) functionalized tQDs (red).

The resulting gels were again mechanically robust (Fig. 3.5A and B) and displayed fluorescence localized to the PLLA-tQD fibers only (Fig 3.5C). Additionally, under uniaxial extension these composites did exhibit the desired reversible red-shift (Fig 3.5D). A striking result from this experiment is that a clear increase in the energy of the tetrapod bandgap occurs with applied strain. Taken at face value, this would mean that stress transfer from the collagen matrix to the electrospun PLLA results in an isotropic compression of the tQD; whereas, when the collagen phase is removed stress is transferred from the PLLA to the tQD in an anisotropic manner. Studies have suggested that polymers do isotropically compress around defect sites during mechanical deformation[23], but it seems unlikely that the addition of collagen would cause such a dramatic change in the microscale deformation mechanisms around the nanoparticle phase. Rather, it is more likely that the idea of a blue-shift being solely attributable to isotropic strain is

overly simplistic. The implications of this result and follow up studies are discussed in more detail in Chapter 4.

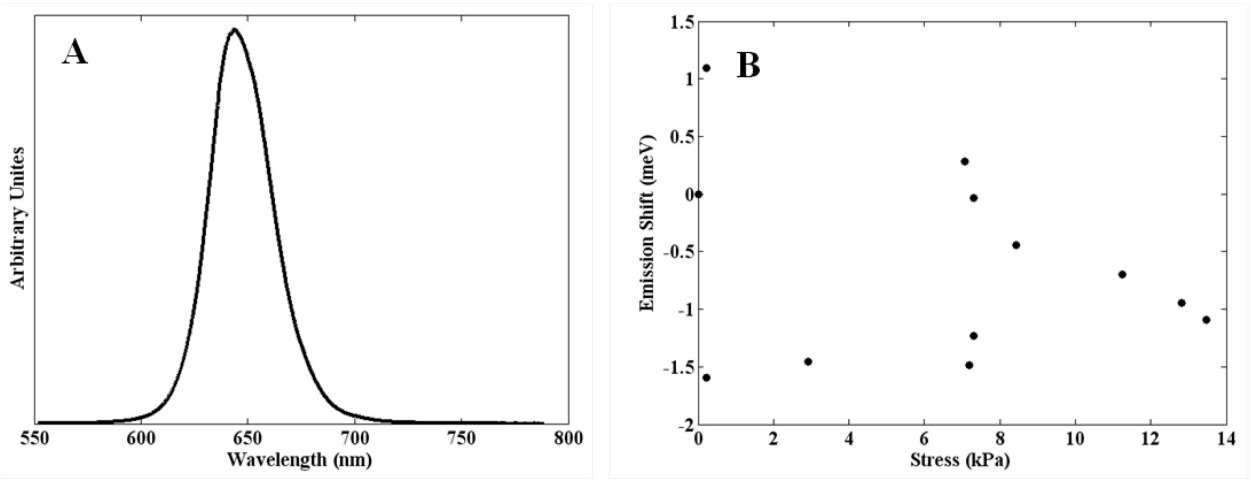


Figure 3.4: Non-responsive behavior of collagen-tQD gels. (A) Fluorescence from tQDs is easily resolvable with high signal to noise even while particles are embedded in gels. (B) No correlation between fluorescence shift and stress measured in gels was observed.

Regardless, as is clear from Figure 3.5 there is a much lower signal to noise ratio than from previous experiments in pure polyer-tQD composites. Again, this can be attributed to the viscous nature of a collagen gel in combination with its relatively low Young's modulus. This does indicated a potential method for probing the strains induced in the collagen matrix by cellular traction forces. In an experiment measuring cellular forces transmitted through this sort of composite, the physiological behavior of the cell would likely be modified as it encounters networks of relatively stiff PLLA fibers. Nonetheless, this offers a relatively simple way to measure cell forces in a three dimensional substrate.

3.4 Future Studies

At this point, the proof-of-concept experiments have been completed. Tetrapods have clearly been demonstrated as a means of accessing difficult to probe mechanical information in the biological environment. However, no specific systems of interest or biological questions have been studies. The following is a potential path forward using the proven capabilities of the tQD to advance understanding of cancer biophysics.

3.4.1 Molecular Restructuring of the ECM

Tumors are directly involved in ECM remodeling and stiffening through several processes including the secretion of MMPs and lysyl oxidase (LOX)[24]. There have been several studies to address the changes in collagen mechanical properties due to crosslinking[12,21,25-27], but none to address the microscale restructuring of the collagen matrix. We will examine the mechanical response of the collagen fibers during the addition of LOX with a dynamic spatial mapping

capability unique to the tQD system. This experiment will be the first to optically probe the microscale effects of collagen crosslinking and their variability throughout a collagen a substrate.

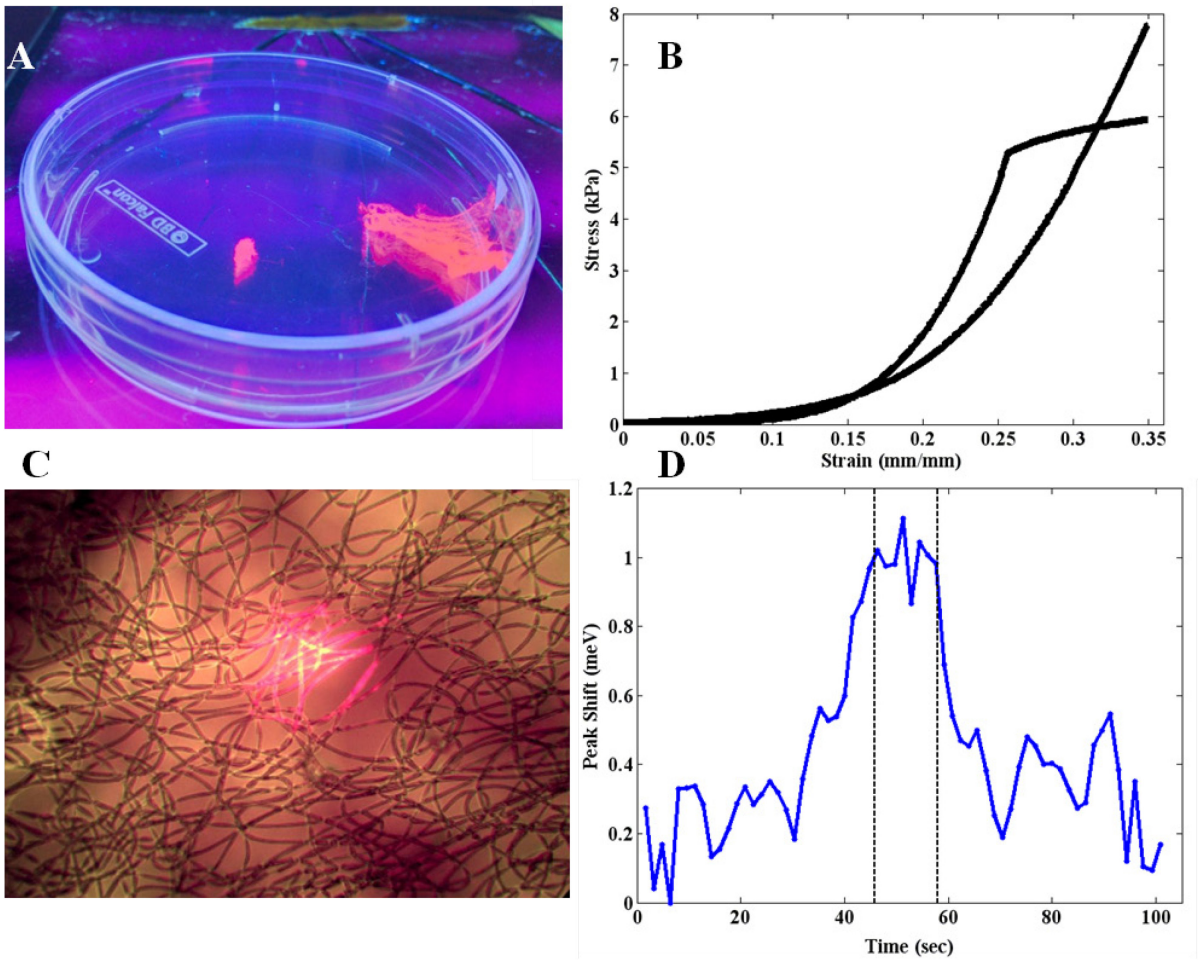


Figure 3.5: Characterization of collage-PLLA-tQD super composites. (A) Picture of fluorescent mats of electrospun PLLA-tQD composite fibers. (B) Example of two stress-strain curves from crosslinked collagen-PLLA-tQD gel composites. (C) tQDs remained localized to fibers (spaghetti-like structures) even after insertion into collagen (background of image). (D) Strain was applied (10-45 seconds, dashed line) and held for 12 seconds (second dashed lined) before being removed.

Although the stiffness of ECM components influences cancer progression, our understanding of the mechanical properties of the main ECM constituent, collagen, is incomplete. In particular, the microdomain stress and strain properties of collagen fibers are unknown. This is important as cancer biologists have been crosslinking fibers by adding chemicals or utilizing enzymes to change the stiffness without a molecular understanding of how they are altering fiber characteristics[18]. Tetrapod quantum dots will enable us to determine the spatial distribution of stresses along perturbed fibers, information that cannot currently be obtained by any other technique. Using the techniques for tQD-composites already demonstrated, fluorescence spectra will be taken along the collagen sample with resolution of 1 μm^2, creating a stress profile as a function of strain. Thus, the relative strain at each spot along the fiber will be quantified for the first time. We will therefore be able to gain a fundamental understanding of collagen mechanics

and dynamics in an unperturbed collagen fiber and the response under an imposed and increasing strain.

Once the basic microscale mechanical properties of the collagen fibers are understood, we can begin to probe biologically important perturbations of the system such as LOX-induced crosslinking. We will examine the mechanical response of the collagen fibers as these factors are introduced into the system. In the simplest experiments, the immediate changes in the mechanical properties of a collagen substrate after incubation with LOX will be examined by optically determining a stress profile along the sample before tensile testing. This will be used to establish any immediate introduction of stresses into the collagen matrix due to crosslinking. The effects of extended incubation with LOX and increased concentrations will be examined.

After establishing a mechanical response to LOX-mediated crosslinking, we will examine how the distribution of strain and polymer chain mobility changes with the application of strain, as larger stresses are present at sites of increasing polymer mobility. This will give the first insights into the heterogeneity of stress during strain in collagen, which will lead to increased understanding of the tissue environment surrounding tumors and how invasive cells are generated.

Alternatives crosslinking agents such as ribose and MMPs could be measured. It is also possible the fluorescence profile of tQDs could be modified by LOX-induced crosslinking of the poly(MAAT) ligand on the nanoparticle surface. A simple control for this is to incubate tQDs with LOX alone and compare fluorescence spectra before and after. Any change could be used as a baseline to be subtracted from further shifts seen in collagen-tQD substrates. Alternatively, if a shift is seen peptide ligands or other functionalities could be used with the tQD.

3.4.2 Biologically Relevant Cell Force Measurements

Cell-generated forces are important for the biology and function of many cell types. For example, during lactation mammary myoepithelial cells generate force on the ECM due to oxytocin-mediated contraction. Cell migration also requires force generation and is important in many diseases including cancer metastasis. Metastasis is a multistage process whereby cancer cells leave the primary tumor site, enter the bloodstream, and seed new organs for tumorigenesis. It is therefore important to quantitatively understand the differences in how normal and tumor cells interact mechanically with their environment and how those differences contribute to the invasive ability of tumor cells. The project proposed in this section will be the first to examine quantitatively the stresses resultant throughout the collagen matrix by normal myoepithelial cells and compare them to myoepithelial/basal cells isolated from tumors. Additionally, the spatial resolution of the tQD system will allow us to examine the restructuring of the collagen matrix in a mechanical frameset during the generation of invasive cells.

Mammary myoepithelial cells (MEC) will be cultured on top of a tQD-functionalized collagen substrate analogous to the studies on cardiomyocytes. This project will use mouse models of human cancer (e.g., MMTV-polyoma virus middle T) as sources of mammary epithelial cells. The nature of the disease is one of the whole organism and requires models that recapitulate all of the cell types, including those that involve complex interactions of cells with their surrounding

environment. Both wild type and transgenic mice that have cell-type specific markers will be used. We will use K14-Actin::GFP mice[28] to mark cells that express K14. Transgenic mice will be mated to inbred mice and continuously backcrossed into the appropriate strain (FVB/n). Transmission of the transgenes will be monitored by analysis of DNA isolated from tail biopsy. GFP-positive cells will be isolated by flow cytometry.

After plating normal myoepithelial cells on a tQD-collagen substrate we will induce contraction. Upon addition of oxytocin, the cell-generated stresses applied to the collagen will be reported by the tQDs. Fluorescence measurements and stress characterization of the resulting film will then be performed with the dynamic and spatial resolutions of the previous experiments. The long term mechanical restructuring of the collagen matrix will also be observed since we will have the capability to maintain a cell line under active observation on our microscope using a CO2, heated stage.

After establishing a baseline for both the magnitude of stress and the spatial distributions of those stresses through collagen by normal MECs, we will culture the corresponding myoepithelial/basal cells derived from tumors on tQD-collagen substrates. Stresses generated through the collagen matrix by oxytocin-induced contraction will again be measured with a corresponding dynamic and spatially resolved stress profile. Again, long term mechanical changes to the substrate will be monitored. To the best of our knowledge, this stress profile will be the first measurement of the differences in the mechanical properties of a collagen matrix due to restructuring of the collagen by tumor cells.

It is well-recognized that tumor cells can modify the ECM by secreting molecules such as matrix metalloproteinases (MMPs)[29]. The Werb lab at UCSF, our collaborators on the cardiomyocytes studies, has developed a full suite of tools to address how MMPs are involved in cell-generated forces including various MMP knockout mice, vectors to over express MMPs, and MMP knockdown constructs. Furthermore, biosensors to measure MMP activity and other protease activity have been developed by the Werb group and others[30]. These tools will allow us to address the questions of how MMPs alter cell-generated forces.

Additionally, we may find that the forces exerted by wild-type and tumor organoids are not different. While this would be a surprising finding given that cancer cells extensively remodel the ECM, this would have far-reaching implications on how we understand the process of tumorigenesis, invasions and metastasis. Therefore, even if we find a negative result we will have learned about the basic mechanisms cancers use to branch and migrate.

Chapter 3 References

1. Alexander, N. R.; Branch, K. M.; Parekh, A.; Clark, E. S.; Iwueke, I. C.; Guelcher, S. A.; Weaver, A. M., Extracellular matrix rigidity promotes invadopodia activity. *Current Biology* 2008, 18, 1295-1299.
2. Engler, A. J.; Griffin, M. A.; Sen, S.; Bönnemann, C. G.; Sweeney, H. L.; Discher, D. E., Myotubes differentiate optimally on substrates with tissue-like stiffness pathological implications for soft or stiff microenvironments. *The Journal of cell biology* 2004, 166, 877-887.
3. Bao, G.; Suresh, S., Cell and molecular mechanics of biological materials. *Nature materials* 2003, 2, 715-725.
4. Choquet, D.; Felsenfeld, D. P.; Sheetz, M. P., Extracellular matrix rigidity causes strengthening of integrin–cytoskeleton linkages. *Cell* 1997, 88, 39-48.
5. Wang, J. H. C.; Lin, J.-S., Cell traction force and measurement methods. *Biomechanics and modeling in mechanobiology* 2007, 6, 361-371.
6. Du Roure, O.; Saez, A.; Buguin, A.; Austin, R. H.; Chavrier, P.; Siberzan, P.; Ladoux, B., Force mapping in epithelial cell migration. *Proceedings of the National Academy of Sciences of the United States of America* 2005, 102, 2390-2395.
7. Pelham, R. J.; Wang, Y.-L., Cell locomotion and focal adhesions are regulated by substrate flexibility. *Proceedings of the National Academy of Sciences* 1997, 94, 13661-13665.
8. Malmström, J.; Christensen, B.; Jakobsen, H. P.; Lovmand, J.; Foldbjerg, R.; Sørensen, E. S.; Sutherland, D. S., Large area protein patterning reveals nanoscale control of focal adhesion development. *Nano letters* 2010, 10, 686-694.
9. Maskarinec, S. A.; Franck, C.; Tirrell, D. A.; Ravichandran, G., Quantifying cellular traction forces in three dimensions. *Proceedings of the National Academy of Sciences* 2009, 106, 22108-22113.
10. Hur, S. S.; del Álamo, J. C.; Park, J. S.; Li, Y.-S.; Nguyen, H. A.; Teng, D.; Wang, K.-C.; Flores, L.; Alonso-Latorre, B.; Lasheras, J. C., Roles of cell confluency and fluid shear in 3-dimensional intracellular forces in endothelial cells. *Proceedings of the National Academy of Sciences* 2012, 109, 11110-11115.
11. Grashoff, C.; Hoffman, B. D.; Brenner, M. D.; Zhou, R.; Parsons, M.; Yang, M. T.; McLean, M. A.; Sligar, S. G.; Chen, C. S.; Ha, T., Measuring mechanical tension across vinculin reveals regulation of focal adhesion dynamics. *Nature* 2010, 466, 263-266.
12. Kreger, S. T.; Bell, B. J.; Bailey, J.; Stites, E.; Kuske, J.; Waisner, B.; Voytik-Harbin, S. L., Polymerization and matrix physical properties as important design considerations for soluble collagen formulations. *Biopolymers* 2010, 93, 690-707.
13. Gupta, H. S.; Seto, J.; Wagermaier, W.; Zaslansky, P.; Boesecke, P.; Fratzl, P., Cooperative deformation of mineral and collagen in bone at the nanoscale. *Proceedings of the National Academy of Sciences* 2006, 103, 17741-17746.
14. Gupta, H. S.; Seto, J.; Krauss, S.; Boesecke, P.; Screen, H. R. C., < i> In situ</i> multi-level analysis of viscoelastic deformation mechanisms in tendon collagen. *Journal of structural biology* 2010, 169, 183-191.
15. Buehler, M. J., Nature designs tough collagen: explaining the nanostructure of collagen fibrils. *Proceedings of the National Academy of Sciences* 2006, 103, 12285-12290.
16. Fratzl, P., *Collagen: structure and mechanics*. Springer New York:: 2008; Vol. 1.

17. Raub, C. B.; Suresh, V.; Krasieva, T.; Lyubovitsky, J.; Mih, J. D.; Putnam, A. J.; Tromberg, B. J.; George, S. C., Noninvasive assessment of collagen gel microstructure and mechanics using multiphoton microscopy. *Biophysical journal* 2007, 92, 2212-2222.
18. Levental, K. R.; Yu, H.; Kass, L.; Lakins, J. N.; Egeblad, M.; Erler, J. T.; Fong, S. F. T.; Csiszar, K.; Giaccia, A.; Weninger, W., Matrix crosslinking forces tumor progression by enhancing integrin signaling. *Cell* 2009, 139, 891-906.
19. Eyre, D. R.; Wu, J.-J., Collagen cross-links. In *Collagen*, Springer: 2005; pp 207-229.
20. Pellegrino, T.; Manna, L.; Kudera, S.; Liedl, T.; Koktysh, D.; Rogach, A. L.; Keller, S.; Rädler, J.; Natile, G.; Parak, W. J., Hydrophobic Nanocrystals Coated with an Amphiphilic Polymer Shell: A General Route to Water Soluble Nanocrystals. *Nano Letters* 2004, 4, 703-707.
21. Castaneda, L.; Valle, J.; Yang, N.; Pluskat, S.; Slowinska, K., Collagen cross-linking with Au nanoparticles. *Biomacromolecules* 2008, 9, 3383-3388.
22. Roeder, B. A.; Kokini, K.; Sturgis, J. E.; Robinson, J. P.; Voytik-Harbin, S. L., Tensile mechanical properties of three-dimensional type I collagen extracellular matrices with varied microstructure. *Journal of biomechanical engineering* 2002, 124, 214-222.
23. Kübel, C.; González-Ronda, L.; Drummy, L. F.; Martin, D. C., Defect-mediated curvature and twisting in polymer crystals. 2000.
24. Kessenbrock, K.; Plaks, V.; Werb, Z., Matrix metalloproteinases: regulators of the tumor microenvironment. *Cell* 2010, 141, 52-67.
25. Puxkandl, R.; Zizak, I.; Paris, O.; Keckes, J.; Tesch, W.; Bernstorff, S.; Purslow, P.; Fratzl, P., Viscoelastic properties of collagen: synchrotron radiation investigations and structural model. *Philosophical Transactions of the Royal Society of London. Series B: Biological Sciences* 2002, 357, 191-197.
26. Rault, I.; Frei, V.; Herbage, D.; Abdul-Malak, N.; Huc, A., Evaluation of different chemical methods for cros-linking collagen gel, films and sponges. *Journal of Materials Science: Materials in Medicine* 1996, 7, 215-221.
27. Deeken, C. R.; Fox, D. B.; Bachman, S. L.; Ramshaw, B. J.; Grant, S. A., Characterization of bionanocomposite scaffolds comprised of amine-functionalized gold nanoparticles and silicon carbide nanowires crosslinked to an acellular porcine tendon. *Journal of Biomedical Materials Research Part B: Applied Biomaterials* 2011, 97, 334-344.
28. Vaezi, A.; Bauer, C.; Vasioukhin, V.; Fuchs, E., Actin cable dynamics and Rho/Rock orchestrate a polarized cytoskeletal architecture in the early steps of assembling a stratified epithelium. *Developmental cell* 2002, 3, 367-381.
29. Pinaud, F.; King, D.; Moore, H.-P.; Weiss, S., Bioactivation and cell targeting of semiconductor CdSe/ZnS nanocrystals with phytochelatin-related peptides. *Journal of the American Chemical Society* 2004, 126, 6115-6123.
30. Jun, Y.-w.; Sheikholeslami, S.; Hostetter, D. R.; Tajon, C.; Craik, C. S.; Alivisatos, A. P., Continuous imaging of plasmon rulers in live cells reveals early-stage caspase-3 activation at the single-molecule level. *Proceedings of the National Academy of Sciences* 2009, 106, 17735-17740.

Chapter 4: Single Particle Studies of Tetrapods

4.1 Fluorescence Studies of Single Tetrapods 38
4.2 Combined AFM-Fluorescence Studies 40
4.2.1 Instrumentation, Procedures, and Pitfalls 41
References 44

4.1 Fluorescence Studies of Single Tetrapods

In order to fully exploit the potential uses of the tQD, we require a more thorough understanding of the fundamental nature of its response. As is evident in Figure 4.1, the fluorescence response is not a purely monotonic shift to lower energy wavelengths with applied strain. Figure 4.1 illustrates examples of how the wavelength shift can involve shoulders (Fig. 4.1A), changes in the full-width half max (FWHM) (Fig. 4.1A), and even shifts to higher energy emission (Fig. 4.1B) in SEBS films (inset). These phenomena all have multiple explanations that can be supported with the current experimental data available.

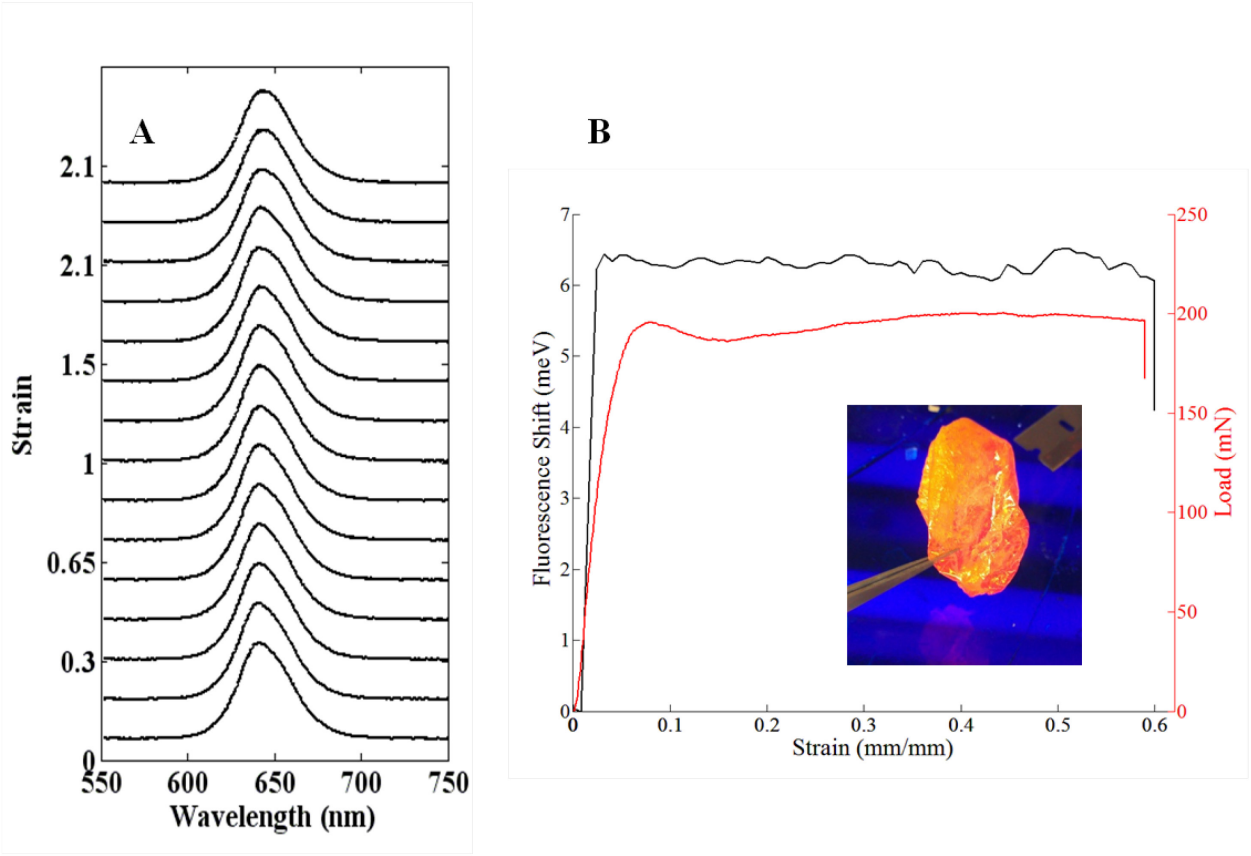


Figure 4.1: Tetrapod fluorescence response exhibits features beyond a simple red-shifting behavior. (A) Normalized fluorescence from a tensile test on a SEBS-tQD composite film (inset of B) shows changes in the FWHM during testing as well as the emergence of shoulders at higher strains. (B) Simultaneous optical and mechanical tests of SEBS-tQD films show increased agreement between mechanical (red) and optical (black) data, but also exhibit a blue-shift in fluorescence.

Shoulders and increases in the FWHM with applied strain could be due to the ensemble nature of the measurement technique. Nanoparticles are being excited over a relatively large area (hundreds of micrometers) compared to their size. Since the internal strain state of a polymer under deformation is clearly not homogenous, the heterogeneity could manifest itself as a broadening of the fluorescence signal as it is the summation of a distribution of strain states or even splitting into shoulders if two particular strain states are dominant in the polymer. Alternatively, changes in the FWHM could be an artifact due to the inherent broadening of the spectral line-width of a single particle under strain[1]. Splitting has also been clearly demonstrated to occur in core-shell particles under high pressures[2-4]. In reality, there is likely to be some confluence of these explanations, but currently it is not possible to predict which the dominant mechanism is.

Similarly, observed red-shifts and blue-shifts can be explained by arguments involving the mechanisms of deformation in the polymer and by how stress is distributed through aggregates of particles regardless of the surrounding polymer deformation. The tQD has been predicted to[5] and experimentally shown[2] to be capable of reporting isotropic and anisotropic pressures as blue-shifts and red-shifts, respectively. In other words, not only can the tQD be used to study stress-transfer as a whole, but could also be used to determine which stress components are nonzero during deformation of the material. If in a polymer composite only one of σ_{11}, σ_{22}, and σ_{33} are nonzero, then particles should experience only a shear, normal, or compressive force. In the case of a compressive force, the resulting tQD shift would be blue with shear and normal forces predicted to result in red shifts. Consequently, particle-composites could be engineered with knowledge of the most likely mode of failure for the particle. This unique capability has yet to be exploited.

Many of these questions can be more fully answered through studies on single particles removed from polymers. In these studies, the ensemble effects are removed and the complexity of the polymer structure is removed. Single particle fluorescence studies of tQDs have already provided insight into how to further develop uses of the tQD.

Previous work has also shown that dual-emission can be detected from single tQDs at room temperature due to lower-probability spatially indirect transitions (Fig. 4.2A)[6]. Typically in CdSe/CdS nanoparticles, recombination occurs entirely in the CdSe from an electron in the LUMO. In spatially indirect transitions, recombination occurs from the LUMO +1 state, which involves an electron in the CdS arms of the tetrapod (Fig. 4.2B). Separately evaluating shifts in the indirect transition and the direct transition could broth provide further insight into the nature of stress transfer to a particle as well as improve the sensitivity of the tQD probe. The current measurement technique involves stress transfer from the polymer to the CdS arm to the CdSe core through the CdSe/CdS lattice interface. Monitoring the indirect transition would essentially involve distortions to the CdS arm directly and presumably increase the response of the probe though the transient nature of the indirect transition would make this difficult (Fig. 4.2C).

However, we currently lack a full understanding of how the tQD‘s optical response depends on force applications at a single particle level. That level of fundamental information can be discovered by employing simultaneous AFM-single particle fluorescence measurements.

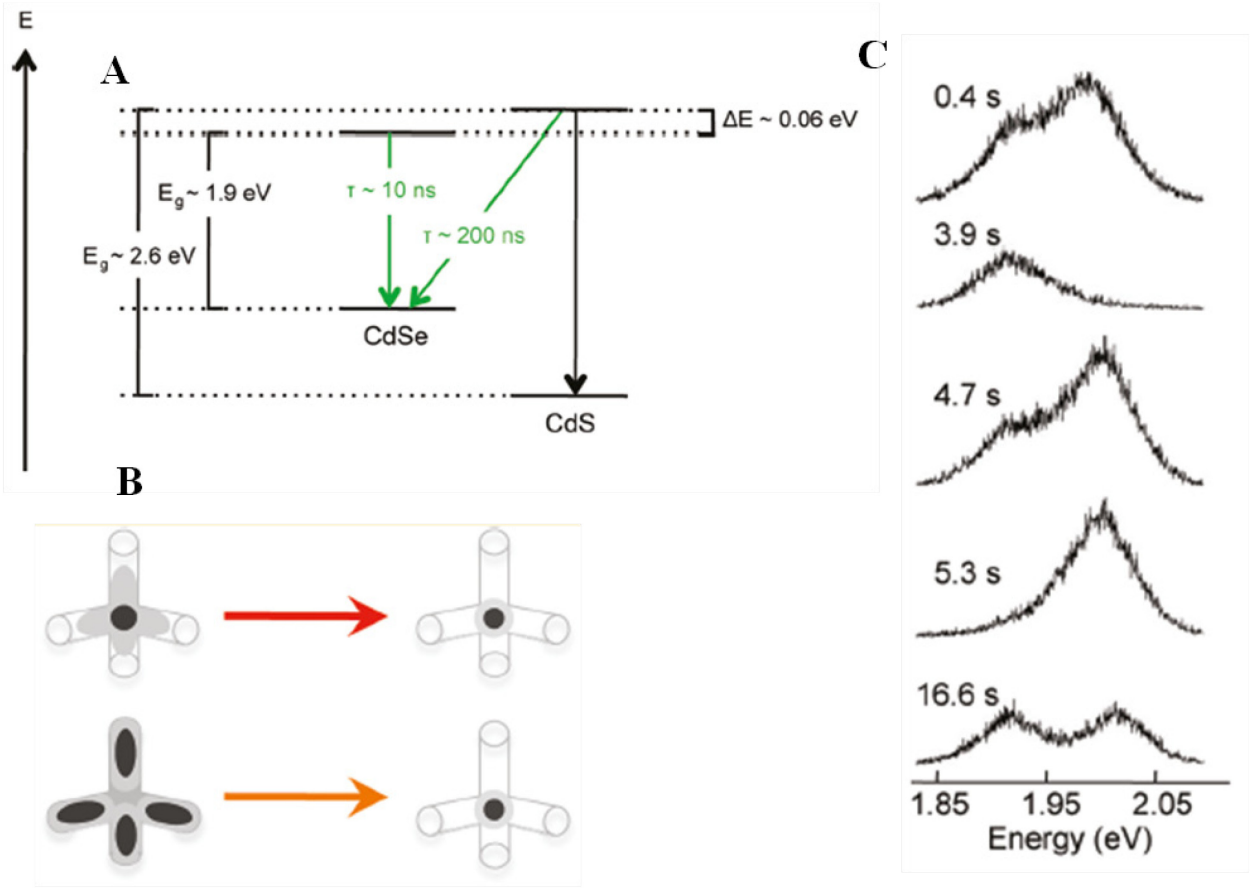


Figure 4.2: Spatially indirect emissive transitions at room temperature in single tQDs. (A) Electronic structure of CdSe/CdS core/shell particles with corresponding differences in radiative lifetimes and energies. (B) Schematic of electron wave function localization (left side) and hole wave function for the observed transitions. (C) Series of spectra from a single tQD over time indicating the transient nature of both the dominant direct transition and less probably indirect transition. Adapted from Reference 6.

4.2 AFM-Fluorescence Measurements

Ideally, a magnitude of shift in tQD emission wavelength could be assigned to a particular force exerted on the nanoparticle. Furthermore, it would be advantageous to be able to differentiate fluorescence shifts from normal, sheer, compressive, and other off axis forces. This set of information would provide us with a fully characterized probe for internal mechanisms of deformation. Currently, we are limited to comparing fluorescence shifts from experiments to a combination of pseudo-empircal predictions[5] and AFM experiments on single CdTe tetrapods[7].

For example, in experiments on the contractile forces of cardiomyocytes fluorescence red shifts of up to -20 meV were observed. By using the predicted effects of uniaxial compression on the lowest energy transitions of CdTe tetrapods, that could be converted to an average contractile force of 0.7 nN. Though that amount of force is consistent with previous reports, there are a number of potential errors in using these sorts of indirect comparisons as calibrations. For example, the DFT calculations were performed on pure CdSe tetrapods with perfectly ordered crystal structures. The tQD is a core/shell particle in which there are likely dislocations, twin boundaries, and other sources of stress concentration.

This experiment will also investigate the fundamental aspects of blue and red shifts that we have observed in the polymer composites. Previous work has shown that polarization anisotropy is observed when tetrapods are cast onto a substrate, breaking the symmetry of the particle[8]. A blue-shift is due to the isotropic compression of the particle and the resulting uniform compression of the bond lengths in the crystal lattice. Consequently, we would expect to observe minimal change in the emission polarization anisotropy of a blue-shifting particle. Conversely, a red-shifting particle should exhibit increased polarization of its emission.

4.2.1 Instrumentation, Procedures, and Potential Pitfalls

These experiments will make use of the unique capabilities of the NT-DMT AFM at LBNL's Molecular Foundry. The NT-DMT microscope is a combination AFM and inverted confocal microscope coupled to an Andor EMCCD. This allows for nanometer resolution optical microscopy with simultaneous AFM measurements of the area of excitation (Fig. 4.3).

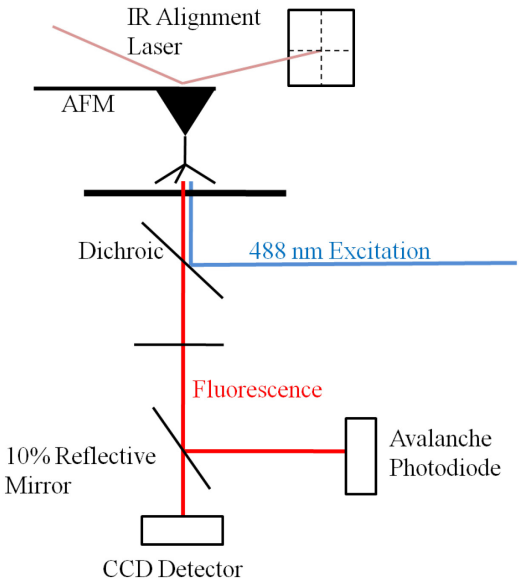


Figure 4.3: Schematic representation of setup for simultaneous AFM and single particle fluorescence measurements.

Tetrapod quantum dots will be synthesized following reported techniques[9-10]. In order to maximize the probability that a point emitter is a tQD, as-synthesized particles will be purified by centrifuging at ~10,000 rpm without the addition of nonsolvent. This technique results in a morphologically pure phase of tQDs at the expense of high yields and is ideal for a single particle experiment. Tetrapods will be dispersed on clean cover glass at a concentration of approximately 1 particle / μm^2 by spin coating a single drop of a 70 pM solution of particles in $CHCl_3$ at 2000 rpm for 1 minute. The resulting coverage should minimize the probability of multiple particles being simultaneous excited or contacted by the AFM.

There are several challenging fluorescence phenomena inherent to single quantum dot experiments that will need to be directly addressed – namely, spectral diffusion and photobleaching. Spectral diffusion (also referred to as walking or wandering) was observed in some of the first single particle CdSe fluorescence studies in the late 1990's[11]. This phenomenon is attributed to the quantum-confined Stark effect as there are nanoscale charge fluctuations in and around the nanoparticle[12-16]. Unfortunately, spectral wandering in CdSe causes fluorescence shifts on the order of 1-10 meV and has the potential to obscure strain induced shifts in single particle experiments. Previously performed proof of concept AFM-fluorescence experiments highlighted this potential problem as well as the ability statistically differentiate the two phenomena (Fig. 4.4).

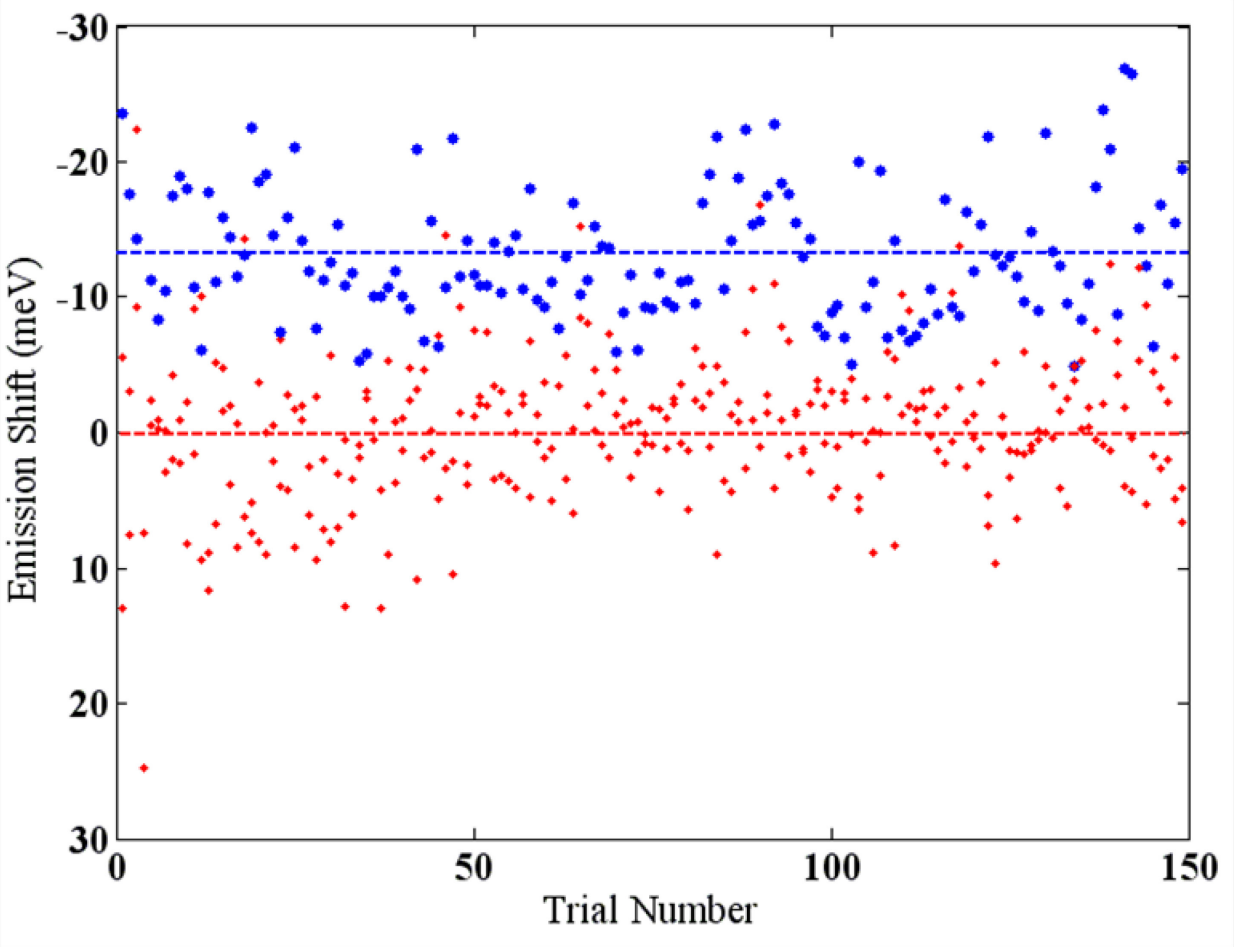


Figure 4.4: Example of spectral wandering in a single tQD (red) as compared to fluorescence shifts (blue). Spectral wandering is a stochastic process that will have a normal distribution of states around a mean value (dashed red line at 0 meV). If induced fluorescence shifts were actually spectral diffusion, subtracting peak emission positions during AFM contact from the mean spectral position during non-contact (dashed red line) should result in the same normal distribution of shifts about a zero mean. However, this treatment in a proof of concept AFM experiment found an average shift of approximate -12 meV (dashed blue line) over several hundred presses ("Trial Number") on single particles. Unfortunately, not corroborating evidence of contact with the tQD could be obtained on the instrument used for this study.

By employing statistically significant periods of time where the AFM tip is in contact and out of contact with the tetrapod, fluorescence shifts can be attributed to the tip-induced strain rather than spectral diffusion. Since spectral diffusion is known to result in a normal distribution of emission wavelengths, a simple t-test can be used to demonstrate that spectral shifts are significantly different during AFM contact and not attributable to diffusion. The length of the in and out of contact periods will be determined by the frame rate of the measurement, such that that number of collected spectra, N, is a statistically relevant size.

However, this measurement is further complicated by photobleaching. Despite having a long life time relative to fluorescent molecules, single tQDs will still photobleach typically over the course of a few minutes of constant excitation. Increased excitation fluence is desirable, because the resulting increased emission allows for more easily resolvable spectra. Conversely, this will decrease the time before a particle photobleaches[17]. Obviously, this makes selecting a excitation intensity a tradeoff between increased statistical significance in differentiating shifts from diffusion and the ability to resolve very small fluorescence shifts in a series of single particle spectra.

Chapter 4 References

1. Empedocles, S. A.; Norris, D. J.; Bawendi, M. G., Photoluminescence spectroscopy of single CdSe nanocrystallite quantum dots. *Physical Review Letters* 1996, 77, 3873-3876.
2. Choi, C. L.; Koski, K. J.; Sivasankar, S.; Alivisatos, A. P., Strain-Dependent Photoluminescence Behavior of CdSe/CdS Nanocrystals with Spherical, Linear, and Branched Topologies. *Nano Letters* 2009, 9, 3544-3549.
3. Akimoto, O.; Hasegawa, H. Strain-Induced Splitting and Polarization of Excitons Due to Exchange Interaction. *Phys. Rev. Lett.* 1968, 20, 916-918.
4. Langer, D. W.; Euwena, R. N.; Era, K.; Koda, T. Spin Exchange in Excitons, the Quasicubic Model and Deformation Potentials in II-VI Compounds. *Phys. Rev. B* 1970, 2, 4005-4022.
5. Schrier, J.; Lee, B.; Wang, L. W., Mechanical and electronic-structure properties of compressed CdSe tetrapod nanocrystals. *J Nanosci Nanotechnol* 2008, 8, 1994-8.
6. Choi, C. L.; Li, H.; Olson, A. C. K.; Jain, P. K.; Sivasankar, S.; Alivisatos, A. P., Spatially indirect emission in a luminescent nanocrystal molecule. *Nano letters* 2011, 11, 2358-2362.
7. Fang, L.; Park, J. Y.; Cui, Y.; Alivisatos, P.; Shcrier, J.; Lee, B.; Wang, L.-W.; Salmeron, M., Mechanical and electrical properties of CdTe tetrapods studied by atomic force microscopy. *The Journal of chemical physics* 2007, 127, 184704
8. Mauser, C.; Limmer, T.; Da Como, E.; Becker, K.; Rogach, A. L.; Feldmann, J.; Talapin, D. V., Anisotropic optical emission of single CdSe/CdS tetrapod heterostructures: Evidence for a wavefunction symmetry breaking. *Physical Review B* 2008, 77, 153303.
9. Talapin, D. V.; Nelson, J. H.; Shevchenko, E. V.; Aloni, S.; Sadtler, B.; Alivisatos, A. P., Seeded growth of highly luminescent CdSe/CdS nanoheterostructures with rod and tetrapod morphologies. *Nano letters* 2007, 7, 2951-2959.
10. Yang, Y. A.; Wu, H.; Williams, K. R.; Cao, Y. C., Synthesis of CdSe and CdTe nanocrystals without precursor injection. *Angewandte Chemie* 2005, 117, 6870-6877.
11. Empedocles, S.; Bawendi, M., Spectroscopy of single CdSe nanocrystallites. *Accounts of chemical research* 1999, 32, 389-396.
12. Empedocles, S. A.; Bawendi, M. G., Quantum-confined stark effect in single CdSe nanocrystallite quantum dots. *Science* 1997, 278, 2114-2117.
13. Empedocles, S. A.; Bawendi, M. G., Influence of spectral diffusion on the line shapes of single CdSe nanocrystallite quantum dots. *The Journal of Physical Chemistry B* 1999, 103, 1826-1830.
14. Galland, C.; Ghosh, Y.; Steinbrück, A.; Sykora, M.; Hollingsworth, J. A.; Klimov, V. I.; Htoon, H., Two types of luminescence blinking revealed by spectroelectrochemistry of single quantum dots. *Nature* 2011, 479, 203-207.
15. Neuhauser, R. G.; Shimizu, K. T.; Woo, W. K.; Empedocles, S. A.; Bawendi, M. G., Correlation between fluorescence intermittency and spectral diffusion in single semiconductor quantum dots. *Physical review letters* 2000, 85, 3301.
16. Shimizu, K. T.; Neuhauser, R. G.; Leatherdale, C. A.; Empedocles, S. A.; Woo, W. K.; Bawendi, M. G., Blinking statistics in single semiconductor nanocrystal quantum dots. *Physical Review B* 2001, 63, 205316.
17. Lee, S. F.; Osborne, M. A., Brightening, blinking, bluing and bleaching in the life of a quantum dot: friend or foe? *ChemPhysChem* 2009, 10, 2174-2191.

Chapter 5: Concluding Remarks

Since the initial verification in 2009 of the theoretical prediction of a CdTe tetrapod's response to uniaxial compression, the tetrapod as a strain gauge has seen remarkable development. Initial experiments in Nylon and polyester fibers affirmed the tQD's ability to sense strain in complex, polymer environments. At the same time, concurrent research on the fluorescence properties of single particles was being performed in order to gain a more thorough understanding of the underlying mechanisms of response.

This work provides further fundamental understanding of how the optical response of a tQD relates to traditional bulk measurements of polymer mechanical properties. The tetrapod allows for the interrogation of failure mechanisms in polymers at a level of detail that has historically been largely inaccessible. At that same time, the foundation for applications to biopolymers and cancer biophysics has been built.

There are many investigations and further developments available for future studies on and utilizing the tQD. For example, it is clear that the tetrapod is useful as a measurement of stress transfer to the particle phase of a nanoparticle-polymer composite. The degree of stress transfer based on interfacial strength (ie, Van der Waals forces vs. hydrogen bonding vs. covalent bonds) is of immediate interest and a natural follow up study to those presented in Chapter 2. Similarly, the ability of the tetrapod to differentiate isotropic from anisotropic strain states has been demonstrated but never utilized. There are many paths forward from this point full with the opportunities for interesting and meaningful results.

Appendix

A1: Methodology for Chapter 2, Tetrapod-Polymer Composites

Synthesis of CdSe-CdS Tetrapods.

CdSe-CdS core/shell tetrapods were prepared in-house via established methods[1-2]. The tetrapods had average arm length 22+-4.5 nm and average diameter 4.0+-0.75.

Preparation of Tetrapod-PLLA Polymer Solutions for Electrospinning.

Poly-L-lactic acid (PLLA, 100,000 g/mol molecular weight) was purchased from ShenZhen ESUN Industrial Co. Ltd., and dissolved in chloroform (Sigma Aldrich) to create solutions of 20% PLLA by weight in chloroform. Tetrapods coated with native hydrophobic ligands (no post-synthetic modification) were dissolved in chloroform and added to the 20% PLLA solution to create solutions of 12% PLLA by weight in chloroform with 3.6%, 10%, 20%, and 40% tetrapods by weight of PLLA.

Electrospinning of Tetrapod-PLLA Composite Single Fibers

Electrospinning was performed using a bias of 15 kV between the collector and syringe needle and collector-syringe needle distance of 15 cm for all runs. For all samples, needles purchased from Nordson corporation (part number 7018225, 38.1 mm gauge length, 0.51 inner diameter) were used. Around 0.1-0.2 mL of solution was loaded into the syringe, and a large droplet of solution was manually ejected immediately prior to turning on the power supplies. Single fibers of diameter 2.5-10 microns were fabricated using the collector design of Li et al (3), consisting of two metal rods of 0.8 cm diameter spaced 9.5 cm apart, while dynamic scanning calorimetry (DSC) samples were fabricated using a random fiber network deposited onto a single metal rod under the same electric field conditions. For transmission electron microscopy (TEM) studies, single aligned fiber arrays were wound around a microtomable epoxy substrate and sputter-coated with 15 nm of gold. Single fibers were removed from the double-rod collector using twisted pipe cleaners coated with double-sided tape, and subsequently taped and glued directly onto the Piezodrive stretcher for fluorescence monitoring or onto small cardboard tabs (10mm x 5mm) for mechanical tests.

Tensile Testing and Optical Diameter Measurements.

Single fibers were removed from the double-rod collector using twisted pipe cleaners coated with double-sided tape, and subsequently taped and glued with epoxy directly onto small cardboard tabs (10mm x 5mm) for mechanical tests. The diameters of the fibers were imaged and photographed using a 63x objective lens on a standard optical microscope (QCapture camera and QImaging software) which was calibrated using a TEM grid (11.85 pixels/micron). The fiber diameters were analyzed using ImageJ.

Tensile testing was performed using an Agilent T150 nanomechanical tensile tester. The strain rate was set to 4e-3 for all runs, and mounted in the tensile tester using standard pivot grips. The

average fiber diameter measured over 20-25 samples was 6.6 ± 2.2, 5.1 ± 0.7, 4.7 ± 2.2 um, and 4.7 ± 1.6 um for 0, 3.6, 10, and 20% tetrapods respectively and the gauge lengths, measured with digital calipers, fell between 6-10 mm. For standard tensile mechanical tests, we conducted a total of 20-25 tests per sample of 0%, 3.6%, 10%, and 20% loading by weight of tetrapods, rods, or dots in the PLLA polymer. For load relaxation tests, performed on five samples for each concentration, the sample was held at a maximum strain of 77% for 53.25 seconds. For hysteresis, performed on five 10% tetrapod-PLA samples, 5 cycles to a maximum strain of 13% were run continuously and the samples had an average diameter of 3.9 um. For modulus calibration, a total of 22 fibers for the 3.6%, 25 samples for the 10%, and 20 samples for the 20% fibers were used.

Piezodrive In Situ Fiber Stretcher

In order to monitor the fluorescence while stretching the single fibers continuously, a piezo-stretcher mounted via screws on a metal platform was used; the platform had a hole to allow the laser to reach the sample. A piezodrive (part number O-103-01) and D-drive controller were purchased from Piezosystems Jena. The piezodrive was controlled using a function generator (Agilent/HP 3314A, 0.001 – 20 MHz) and the triangle wave signal was monitored using a 500 MHz oscilloscope. The gauge length for all optical tests was 1.8 mm. The piezodrive was calibrated to move at a strain rate of approximately 4e-3 for all tests. Strain was calculated by dividing the total range of motion of the drive by the fiber gauge length. The piezodrive was screw-mounted on a 0.5” steel platform (6x8”) with a hole for laser passage for stability during stretching.

For hysteresis, a maximum strain of 13% was used, and a total of four cycles were run per sample, while for load relaxation, a maximum strain of 77% was used and one cycle was run per sample, and the sample was held at the maximum strain for 53.25 seconds.

The nanocrystal fluorescence was excited with a 488-nm Ar+ laser (Lexel Laser, Inc., 95) with 1-W power and 250-μm spot size at the sample. Brightfield and fluorescence images were taken with a digital microscope camera (Paxcam 2+). The fluorescence spectra were monitored using a home-built inverted fluorescence microscope with a spectrometer (Acton Research Corporation, SpectraPro-3001) and CCD detector (Princeton Instruments, Model 7509-0001). Exposure times of 1 s were used to collect spectra with a 0.6 s lag time between frames. Approximately 190 spectra were collected for each load relaxation curve and 220 for each series of 4 loading cycles. Fluorescence spectra were collected over the area of the laser spot and fit to single Gaussians. Change in emission was defined as the difference between the peak position at time t and the peak position at zero strain. Stress relaxation rates were determined by fitting the emission shift versus time to a single exponential decay: $\Delta Emission(t) = Ae^{-\lambda t}$. For mechanical tests, stress was substituted for emission shift. Optical decays were fit to a series of 35 spectra over 53 sec. Mechanical decays were fit to approximately 530 load measurements over 53 sec. Optical stress relaxation data was collected on 13, 14 and 12 fibers of 3.6%, 10%, and 20% tetrapod load by weight, respectively.

Transmission Electron Microscopy Imaging and Sample Preparation

Epoxy (Araldite 502, Electron Microscopy Sciences) was formed into a thin plate by curing overnight at 60C in a shallow dish. The electrospun fibers sample were then wrapped around these substrates and sputter -coated with around 15-20 nm of gold using a Desktop II Denton sputter coater. They were then embedded in more epoxy stained with rhodamine 6G (Sigma Aldrich) and cured overnight at 60C. Thin sections approximately 60 nm in thickness were cut using an RMC MT-X Ultramicrotome (Boeckler Instruments) and picked up from water onto copper TEM grids. The thin sections were imaged using an FEI Tecnai 12 at an accelerating voltage of 120keV or an FEI Tecnai G2 at an accelerating voltage of 200keV.

Supplemental Figures

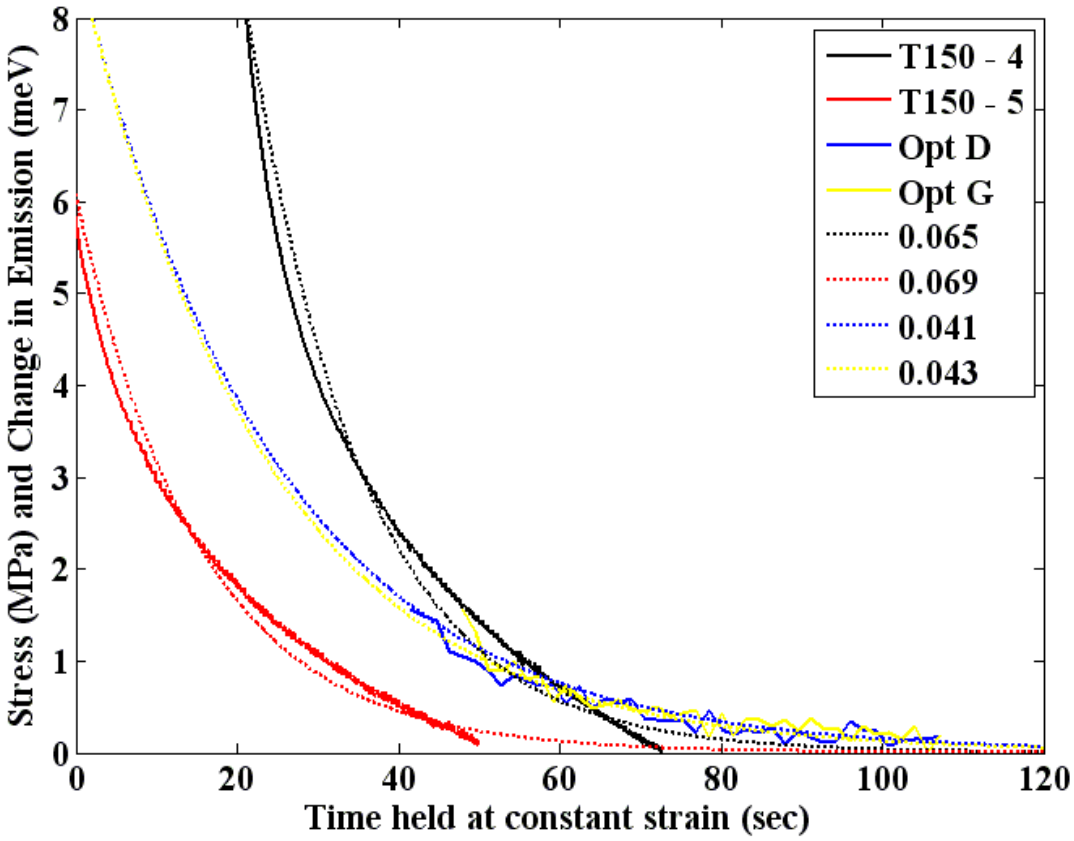


Figure A1.1: Stress relaxation curves from PLLA-tQD tensile trials fit to single exponential decay functions. The legend indicates the decay time in seconds for each fit. Optical decays (yellow and blue) were found to be much faster than mechanically measured decay (black and red).

Table A1.1 – Optical response and particle concentration

Samples	Loading (Weight Percent)	Mean Slope	Min Slope	Max Slope	Young's Modulus (GPa)	Max Shift Std	Stress Shift (Max Shift/Young's Modulus) (meV/GPa)
13	3.60%	0.39±0.2	0.11	0.77	1.9±0.5	9.54±3.82	5.02±0.55
14	10%	0.58±0.29	0.25	1.2	1.7±0.4	12.42±5.2	7.3±1.1
12	20%	0.62±0.24	0.31	0.97	2.5±0.75	11.3±2.0	4.5±0.43
				Average stress shift, over all concentrations:			5.61±0.7

Mechanical properties of PLLA-tQD and SEBS-tQD composites

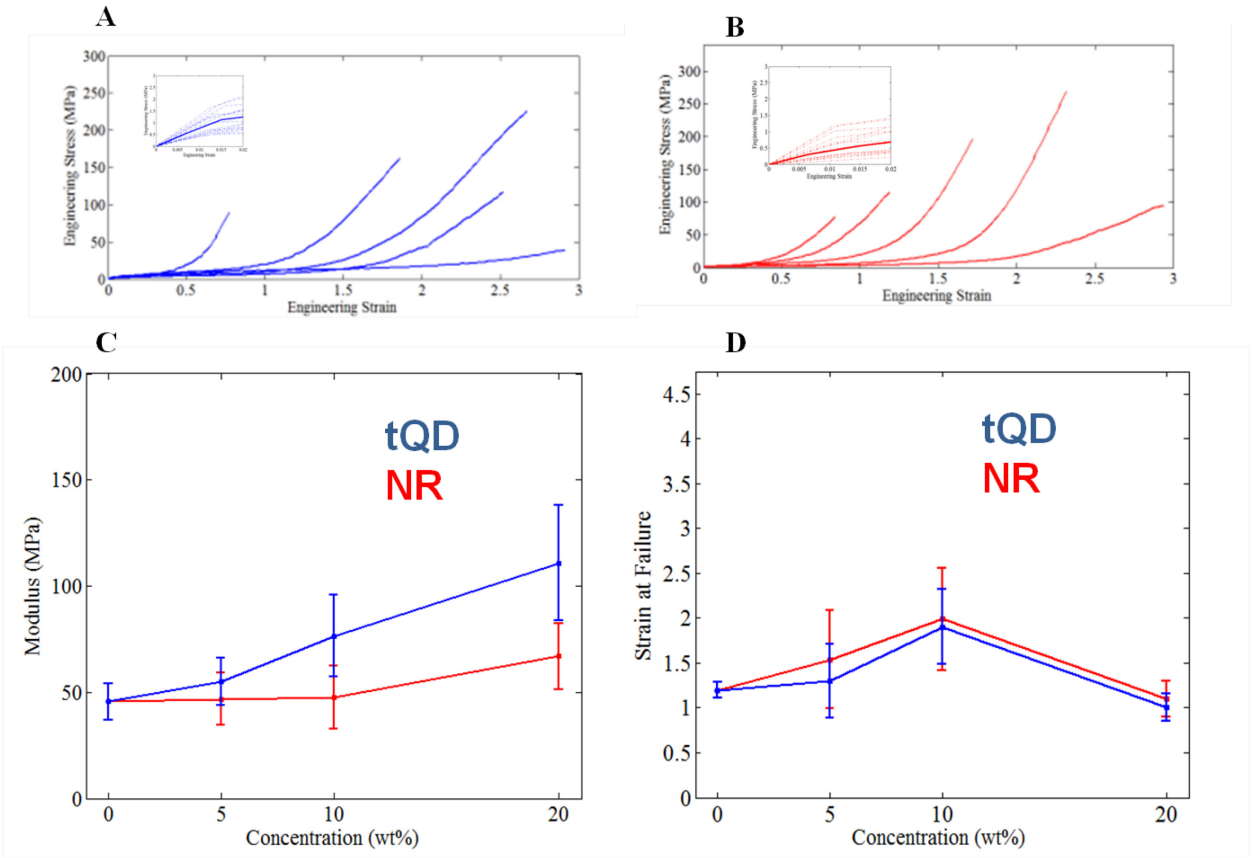


Figure A1.2: Mechanical properties of SEBS-nanoparticle composites. (A and B) Representative tensile tests to failure for SEBS-tQD (A) and SEBS-nanorod (B) electrospun fibers. (C) Measured modulus of SEBS-nanoparticle fibers. tQDs were shown to enhance the composite modulus to a great extent than nanorods at all measured volume fractions. (D) Strain at failure for composites did not follow any clear trends or vary with a great deal of statistical significance.

Table A1.2: Mechanical properties of PLLA-tQD fibers

Particle % by weight	0%	3.6%	10%	20%	40%
Modulus (GPa)	2.2±0.4 (27 samples)	1.9±0.5 (20 samples)	1.7±0.4 (21 samples)	2.47±0.75 (20 samples)	2.070±0.4(6 samples)
Toughness(MPa)	51.52±33.2	38.8±19	46.9±31.9	48.6±25.5	21.73±15.8
Strain at Failure (mm/mm)	1.05±0.86	0.58±0.31	1.25±0.87	0.854±0.411	0.65±0.48
Stress at Failure (MPa)	84±48.6	103.2±33.5	54.22±26.56	73.32±29.8	38.55±18.9
Specimen Diameter (um)	8.9±4.8	5.10±7.4	5.3±2.6	5.46±1.7	4.76±1.62
Number of Samples Tested	27	15	16	15	6

Appendix References

1. Talapin, D. V.; Nelson, J. H.; Shevchenko, E. V.; Aloni, S.; Sadtler, B.; Alivisatos, A. P., Seeded growth of highly luminescent CdSe/CdS nanoheterostructures with rod and tetrapod morphologies. *Nano letters* 2007, 7, 2951-2959.
2. Yang, Y. A.; Wu, H.; Williams, K. R.; Cao, Y. C., Synthesis of CdSe and CdTe nanocrystals without precursor injection. *Angewandte Chemie* 2005, 117, 6870-6877.